



A Concurrent Multi-Process Refinement method applied in two-dimensional strong-coupled fluid-structure interaction problems

Hao Qin^{a,c,d}, Lin Mu^{a,b,c,d,*}, Wenyong Tang^e, Zhe Hu^f

^a College of Marine Science and Technology, China University of Geosciences, Wuhan, 430074, China

^b College of Life Sciences and Oceanography, Shenzhen University, Shenzhen, 518057, China

^c Southern Marine Science and Engineering Guangdong Laboratory (Guangzhou), Guangzhou, 511458, China

^d Shenzhen Research Institute, China University of Geosciences, Shenzhen, 518057, China

^e State Key Laboratory of Ocean Engineering, Shanghai Jiao Tong University, Shanghai, 200240, China

^f Key Laboratory of Ships and Ocean Engineering of Fujian Province, Jimei University, Xiamen, 361021, China

ARTICLE INFO

Keywords:

Refinement method
Fluid-structure interaction
Monolithic FSI method
Liquid sloshing
Dam breaking impact
Wave slamming

ABSTRACT

A Concurrent Multi-Process Refinement method for fluid-structure interaction (FSI) problems is developed and applied in a SIMPLE-based monolithic implicit method (SBMIM) initially presented by Hu et al. (2016). Concurrent Multi-Process Refinement method refines the computational domain of FSI simulations as several sub-domains in multi-processes with multi-grid sizes and multi-time steps. Through file mapping, velocity and pressure data are transmitted between two processes using proper interpolations and time advance strategy. Numerical implementation and algorithm procedure of the method are explained in detail. Simulations of the liquid sloshing in a baffled tank are conducted to give an error estimation on different grid systems using the Grid Convergence Index (GCI). Simulations of the dam breaking flow slamming a vertical wall are conducted to verify the accuracy of present methods and to discuss the area selection of the localized FSI simulation. Simulations of the green water impact caused by freak wave are conducted to show the performance of this method in dealing with multi-scale ocean engineering problems and high-frequency structural vibrations. From results, it is seen that Concurrent Multi-Process Refinement method shows advantages in multi-scale FSI simulations using monolithic FSI methods and in predicting high-frequency structural vibrations, especially with low-cost computational facilities.

1. Introduction

Numerical simulation of fluid-structure interaction (FSI) has quite a range of applications in scientific and engineering fields, e.g., aeroelastic problems (Farhat et al., 2006; Yao and Marques, 2017; Ilie, 2018; etc.), hydroelastic problems (De Rosi et al., 2014; Sun et al., 2015; Hu et al., 2016; etc.) and hemodynamic problems (Torii et al., 2009; Kamensky et al., 2015; Chen and Luo, 2018; etc.). With the development of computational facilities and multi-physics theories, numerical simulations of FSI problems are widely conducted in different scientific and engineering fields nowadays, which save a large amount of physical experiment costs and bring in much convenience to researchers. As such, different numerical methods have been developed to model various coupled FSI phenomena when FSI effects are non-negligible.

From the perspective of discrete strategy, FSI methods can be

categorized into mesh-based methods and meshless method. On one aspect, mesh-based methods are widely used as the numerical approaches in dealing with FSI problems, in which the computational domain is discretized by a set of grids or meshes and the governing equations are solved by numerical schemes such as the Finite Volume Method (FVM), Finite Difference Method (FDM) and Finite Element Method (FEM). Firstly, it is called a fully-Eulerian method if the meshes are fixed in space, in which additional techniques should be used to capture the free surface, such as Volume of Fluid (VOF) and Level Set (LS) (Wick, 2013; Richter, 2013; Cottet and Maitre, 2016; Hu et al., 2016; etc.). Generally speaking, fully-Eulerian method using interface-capturing methods such as VOF is accurate and suitable for complex geometry deformation such as violent free surface evolutions, however, it requires solution of additional equations to capture the free surface interface and thus increases the numerical complexity. Secondly,

* Corresponding author. College of Marine Science and Technology, China University of Geosciences, Wuhan, 430074, China.

E-mail addresses: qh1qh100@alumni.sjtu.edu.cn (H. Qin), moulin1977@hotmail.com (L. Mu).

<https://doi.org/10.1016/j.oceaneng.2019.106912>

Received 12 July 2018; Received in revised form 17 December 2019; Accepted 29 December 2019

Available online 9 January 2020

0029-8018/© 2019 Elsevier Ltd. All rights reserved.

it is called an Arbitrary Lagrangian Eulerian (ALE) method if moving meshes are used to track the changing free surface, in which the meshes move independently to track the free surface interface deformation (Farhat and Lakshminarayan, 2014; Wu and Cai, 2014; Basting et al., 2017; Calandrini and Aulisa, 2019; etc.). Space-Time method is another kind of moving mesh strategy to track free surface, in which the time variable is treated as an additional spatial coordinate to solve the governing equations over a generalized space-time domain (Takizawa and Tezduyar, 2011; Bazilevs et al., 2013; etc.). The interface-tracking methods such as ALE and Space-Time show advantage in the accuracy of capturing moving fluid-structure interface, while they suffer mesh distortion when the free surface changes dramatically. Thirdly, Boundary Element Method (BEM) is the other kind of mesh-based method to simulate FSI problems, except that the computation domain is only meshed at the free surface and fluid-structure interface (Zhang et al., 2013; Rodríguez-Tembleque et al., 2015; Ravník et al., 2016; Heltai et al., 2017; etc.). However, BEM is usually limited to relatively simple geometries and physics, which makes it hard to handle strong nonlinear phenomena such as wave breaking and slamming.

Moreover, meshless methods such as Smoothed Particle Hydrodynamics (SPH) method and Moving Particle Semi-implicit (MPS) method have found their way in recent years in dealing with FSI problems involving complex and nonlinear free surface evolutions. Since the fluid and structure particles follow exactly the motion within a fully-Lagrangian frame, and thus meshless methods are also called the particle methods. SPH method works by dividing the fluid and structure into a set of discrete moving particles that follow the N-S equations and handling particle-particle interaction through a kernel function (Yang, 2011; Liu et al., 2013; Hu et al., 2014; Li et al., 2015; Fourey et al., 2017; etc.). MPS method is similar to the SPH method, yet it applies simplified differential operator models solely based on a local weighted averaging process without taking the gradient of a kernel function (Mitsume et al., 2014; Hwang et al., 2014; Sun et al., 2015; Hwang et al., 2016; Zhang and Wan, 2018; etc.). Meshless methods such as the SPH and MPS have advantages in describing violent free surface evolutions and avoiding distortion of meshes. However, meshless methods usually have difficulty in setting boundary conditions and suffer computational inefficiency compared to mesh-based methods.

From the perspective of coupling strategy, FSI methods can be categorized into partitioned FSI methods and monolithic FSI methods. Partitioned FSI methods solve the fluid and structure domains in partitioned solvers and interactively link them with appropriate coupling approaches (Farhat and Lesoinne, 2000; Matthies and Steindorf, 2003; Küttler and Wall, 2008; Liu et al., 2014; etc.). Partitioned FSI methods are popular among researchers due to the reason that they take the best advantages of existing fluid solvers (Fluent and Star-CCM+ for example) and structure solvers (ANSYS and ABAQUS for example). Besides, partitioned FSI methods are relatively simple in theory and easy for programming, and they perform well for weak-coupled FSI problems. However, partitioned FSI methods might suffer from the problem of computational instability and inaccuracy for strong-coupled FSI problems. Monolithic FSI methods solve the fluid and structure domains simultaneously in a fully coupled way, in which the fluid and structure domains are combined to form a monolithic relation through fluid-structure interface boundary conditions (Le Tallec and Mouro, 2001; Hübner et al., 2004; Heil et al., 2008; Hu et al., 2016; etc.). Using monolithic FSI equations, monolithic FSI methods have shown advantages in computational stability, efficiency as well as the accuracy for strong-coupled FSI problems.

Although monolithic FSI methods are favorable for the stability and efficiency of calculation, they lose the advantage of efficiency under certain conditions. Since the complete system of nonlinear algebraic equations that formed from the coupled governing equations of the fluid and structure domains are solved as a whole, monolithic FSI methods are usually believed to be too computational expensive for use in large-scale or multi-scale problems (Förster et al., 2007; Heil et al., 2008). In other

words, when the simulation domain (fluid domain mainly) is large, monolithic methods have to solve the coupled equations in the whole domain at every single time step. Additionally, it is well acknowledged that usually, calculation of the structure domain requires a much smaller time step compared to the fluid domain, so that the high-frequency structural vibration of metal structures can be captured precisely using a high sampling frequency. However, the time step for the fluid and structure domains applied in monolithic FSI methods are usually the same, increasing the simulation cost enormously. Moreover, although many researchers have contributed a great deal in the cost-saving of the computational fluid dynamics (CFD) simulations using refinement methods (Löhner, 2001; Plewa et al., 2005; Ahmed and John, 2015; Fernández-Tena et al., 2017; etc.) and parallel computing methods (Gropp et al., 2001; Amritkar et al., 2014; Crespo et al., 2015; Afzal et al., 2017; etc.), methods on improving efficiency of monolithic FSI methods are still in need of investigation, especially using low-cost computational facilities.

The origin of coupling problems can well be explained by the fluid added mass, the significance of which determines whether a strong coupling is required or whether a weak coupling suffices. To solve significant added mass issues, Hu et al. (2016) presented a SIMPLE-based implicit method (SBMIM) for the strong coupling of FSI, which was validated and proved to be stable and robust under extreme simulation circumstances. However, several problems were found on the computational efficiency when the simulation is conducted in multi-scale, and when the vibration frequency of the structure is high. Based on SBMIM, a Concurrent Multi-Process Refinement method is developed to solve the computational efficiency problems in this study. For multi-scale problems, the structure mainly interacts with the fluid nearby, and the far-away fluid adds little to the interaction. Therefore, Concurrent Multi-Process Refinement method split the fluid in two parts: the nearby fluid and the far-away fluid. The nearby fluid is solved simultaneously with the structure, forming the Local Process. The far-away fluid is solved using a weak coupling with the nearby fluid, forming the Main Process. In this way, simulations of the nearby fluid and the far-away fluid can be conducted concurrently in multi-processes, localizing the FSI simulation area. Moreover, different grid sizes and time steps can be applied in multi-processes, overcoming the difficulty of using monolithic FSI method when very small time step is required by high-frequency structural vibrations of metal structures. Through file mappings on the computer's memory, data of velocity and pressure variables are transmitted between multi-processes on the Fluid-Entry Boundary using Dummy Grid with proper interpolations and time advance strategy. In order to show the performance of Concurrent Multi-Process Refinement method, two refinement studies are carried out, namely a liquid sloshing case and a dam breaking impact case. Simulations of the liquid sloshing in a baffled tank are conducted to give an error estimation regarding grid sizes and time steps using a GCI method. Simulations of the dam breaking flow slamming a vertical wall is conducted to verify the accuracy of present methods and to discuss the selection of localized FSI simulation area. Simulations of the green water impact a deck-house caused by freak wave are conducted to show the performance of the method in balancing accuracy and efficiency when dealing with practical multi-scale ocean engineering problems with high-frequency structural vibrations. Through the three validation and application cases, it is seen that Concurrent Multi-Process Refinement method shows advantages in multi-scale FSI simulations using monolithic FSI methods and in prediction of high-frequency structural vibrations. Through the calculations of the added mass in the dam breaking case and the green water impact case, it is also seen that the method is quite stable and robust for strong-coupled FSI issues, in which the added mass is significant.

By applying Concurrent Multi-Process Refinement method, the efficiency and accuracy of FSI simulations are balanced and improved, especially for FSI simulations using low-cost computational facilities like ordinary personal computers. Pure-CFD simulations which solves the

N-S equations and FSI simulations which solves the strong-coupled FSI equation are divided in multi-processes. Different grid sizes and time steps can be applied in multi-processes concurrently to meet the accuracy requirement of strong-coupled FSI area and the efficiency requirement of the others. More importantly, the very small time step required by the high-frequency structural vibrations can be avoided in the Pure-CFD processes where FSI plays a negligible role. However, it needs to mention that since the basic idea of Concurrent Multi-Process Refinement method lies in the splitting of the fluid domain, the area selection of Local Process should be careful so that the origin of strong coupling (e.g. the added mass) would not be under-estimated.

$$[2\mathbf{M}/\Delta t^2 + 11\mathbf{C}/(6\Delta t) + \mathbf{K}]\mathbf{w}^{t+\Delta t} = \mathbf{F}^{t+\Delta t} + (5\mathbf{M}/\Delta t^2 + 3\mathbf{C}/\Delta t)\mathbf{w}^t - [4\mathbf{M}/\Delta t^2 + 3\mathbf{C}/(2\Delta t)]\mathbf{w}^{t-\Delta t} + [\mathbf{M}/\Delta t^2 + \mathbf{C}/(3\Delta t)]\mathbf{w}^{t-2\Delta t} \quad (2.8)$$

2. Fluid-structure interaction method

2.1. Governing equations

The fluid refers to liquid, which is assumed to be viscous, Newtonian and incompressible. By applying the VOF-Youngs method (Youngs, 1982) to reconstruct the free surface, governing equations of the fluid include the continuity equation, the momentum conservation equation and the fluid volume transportation equation, written as follows:

$$\nabla \cdot (\theta \mathbf{u}) = 0 \quad (2.1)$$

$$\partial \mathbf{u} / \partial t + \nabla \cdot (\mathbf{u} \otimes \mathbf{u}) = \nabla \cdot \boldsymbol{\sigma}^f / \rho^f + \mathbf{f}^f \quad (2.2)$$

$$\partial(\theta F^f) / \partial t + \nabla \cdot (\theta \mathbf{u} F^f) = 0 \quad (2.3)$$

where \mathbf{u} , ρ^f , \mathbf{f}^f and $\boldsymbol{\sigma}^f$ are the velocity, density, body force and Cauchy stress tensor of the fluid. F^f denotes the transportation volume of the fluid, while the ratio of the volume occupied of fluid is described by θ , which equals 1 where fluid can flow across the mesh boundary freely and 0 where the mesh boundary is solid (Lin, 2007).

Governing equation of the structure is given by the structure momentum equation:

$$\rho^s \ddot{\mathbf{w}} = \nabla \cdot \boldsymbol{\sigma}^s + \mathbf{f}^s \quad (2.4)$$

where \mathbf{w} , ρ^s , \mathbf{f}^s and $\boldsymbol{\sigma}^s$ are the displacement, density, body force and first Piola-Kirchhoff stress tensor of the structure.

On the fluid-structure interface, velocity and traction force of the fluid domain must agree with the structure domain:

$$\mathbf{u} = \dot{\mathbf{w}} \quad (2.5)$$

$$\boldsymbol{\sigma}^f \mathbf{n}^f = \boldsymbol{\sigma}^s \mathbf{n}^s \quad (2.6)$$

where \mathbf{n}^f and \mathbf{n}^s are the unit outward normal vector of the fluid boundary and the unit outward normal vector of the structure boundary.

2.2. Fluid-structure coupling

A self-developed solver is utilized for FSI simulations, which solves the incompressible Navier-Stokes (N-S) equations under two-dimensional flow conditions in CFD simulations, and solves the monolithic FSI equation in FSI simulations.

Finite element method (FEM) is used to discretize two-dimensional Euler beams simplified from structures that meet the cylindrical bending assumption (Timoshenko and Woinowsky-Krieger, 1959). The structure here is assumed to be under small displacement and within the

elastic range. The structural dynamic equation can be written as:

$$\mathbf{M}\ddot{\mathbf{w}} + \mathbf{C}\dot{\mathbf{w}} + \mathbf{K}\mathbf{w} = \mathbf{F} \quad (2.7)$$

where \mathbf{M} is the global matrix of mass, \mathbf{C} is the global matrix of damping, \mathbf{K} is the global matrix of stiffness, \mathbf{F} is the nodal force vector. Implicit Houbolt scheme (Houbolt, 1950), which has been proved unconditionally stable (Newmark, 1959; Johnson, 1966; Nickel, 1971), is used to calculate the structural velocity and acceleration at time $t + \Delta t$ with time step Δt , and thus Eq. (2.7) is rewritten as:

From Eqs. (2.5) and (2.6), the relation between fluid velocity $\mathbf{u}_{couple}^{t+\Delta t}$ on the fluid-structure interface and structure displacement \mathbf{w} , and the relation between the structure nodal force $\mathbf{F}^{t+\Delta t}$ and fluid pressure $\mathbf{P}_{couple}^{t+\Delta t}$ on fluid-structure interface are given as:

$$\mathbf{u}_{couple}^{t+\Delta t} = \mathbf{A}_{couple_1} \mathbf{w}^{t+\Delta t} \quad (2.9)$$

$$\mathbf{F}^{t+\Delta t} = \mathbf{A}_{couple_2} \mathbf{P}_{couple}^{t+\Delta t} \quad (2.10)$$

where \mathbf{A}_{couple_1} and \mathbf{A}_{couple_2} are the conversion matrices generated in coupling calculation. Note that on fluid-structure interface, only the pressure-related force is considered. Viscous effect is neglected at fluid-structure interface since it plays an unimportant role in the simulation cases that this FSI method is designed for.

SIMPLE method (Patankar and Spalding, 1972) is used to solve the fluid governing equations. Finite difference method (FDM) is used to discretize the fluids, while a fixed staggered-grid (Eulerian grid) system is used within which the pressure is defined at the grid center and the velocity is defined at the grid boundaries' center. Central difference scheme (CDS) is used for the pressure gradients and diffusion terms, and the combination of the central difference and upwind difference scheme (UDS) is used for advection terms.

Using a two-step projection method on Eq. (2.2), tentative velocity is expressed as:

$$(\tilde{\mathbf{u}}^{t+\Delta t} - \mathbf{u}^t) / \Delta t = \mathbf{f}^{f,t+\Delta t} + [\nu \nabla^2 \mathbf{u}^t - \nabla \cdot (\mathbf{u}^t \otimes \mathbf{u}^t)] \quad (2.11)$$

where ν is the kinematic viscosity, $\tilde{\mathbf{u}}^{t+\Delta t}$ is the tentative velocity at time $t + \Delta t$, \mathbf{u}^t is the true velocity at time t . The tentative velocity is further updated as the true velocity with the use of correct fluid pressure at time $t + \Delta t$ using relation as:

$$\frac{(\mathbf{u}^{t+\Delta t} - \tilde{\mathbf{u}}^{t+\Delta t})}{\Delta t} = - \frac{\nabla p^{t+\Delta t}}{\rho^f} \quad (2.12)$$

where $p^{t+\Delta t}$ is the fluid pressure at time $t + \Delta t$, obtained by solving pressure Poisson equation as:

$$\nabla^2 \left(\theta \frac{p^{t+\Delta t}}{\rho^f} \right) = \nabla \cdot \left(\theta \frac{\tilde{\mathbf{u}}^{t+\Delta t}}{\Delta t} \right) \quad (2.13)$$

Here, fluid pressure $p^{t+\Delta t}$ in Eq. (2.13) can be solved using a successive over relaxation (SOR) method.

For the fluid grids with fluid-structure interfaces on their boundaries, the interfaces can be treated as mobile solid boundaries (Hu et al., 2016), therefore, the SIMPLE-based pressure Poisson equation can be modified by replacing the tentative velocity in Eq. (2.13) with the mobile solid boundary velocity:

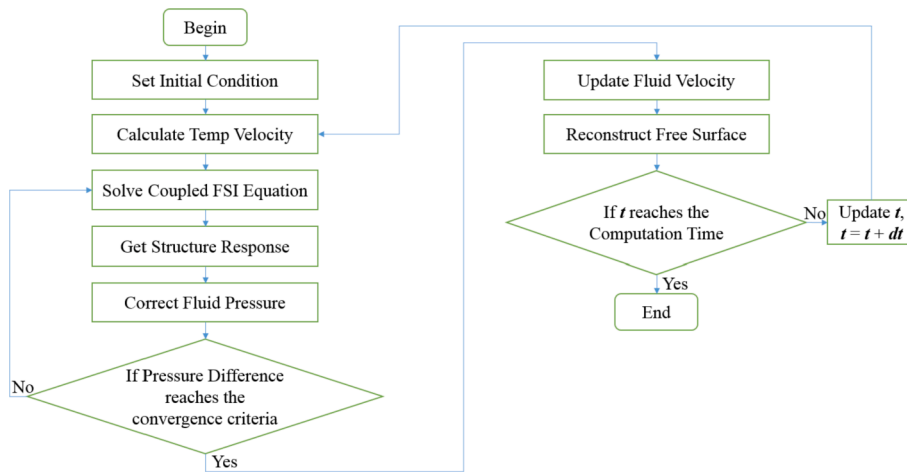


Fig. 1. Flow chart of the SIMPLE-based monolithic implicit method.

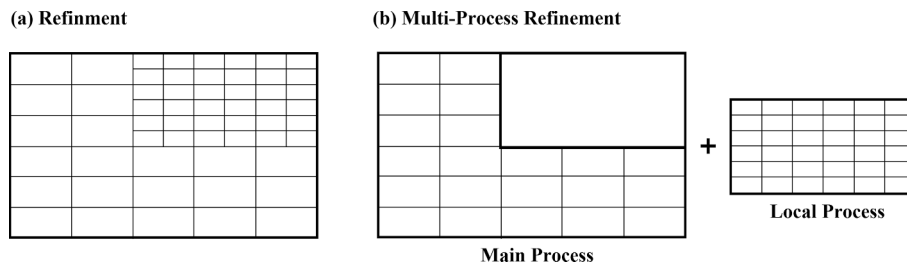


Fig. 2. Comparison of traditional refinement and Multi-Process Refinement method.

$$P_{couple}^{t+\Delta t} = B_{couple} \left(u_{couple}^{t+\Delta t} \right) \quad (2.14)$$

where B_{couple} is the conversion matrix function formed in coupling calculation.

Through simultaneous equations of Eq. (2.9), Eq. (2.10) and Eq. (2.11), structure nodal force is obtained as:

$$F^{t+\Delta t} = A_{couple_2} B_{couple} \left(A_{couple_1} w^{t+\Delta t} \right) \quad (2.15)$$

Combining Eq. (2.15) with Eq. (2.8), the coupled structural dynamic equation is written as:

- (2) At each time step of the FSI simulation, tentative velocity of the fluid is obtained in module ‘Calculate Temp Velocity’ using a two-step projection following the SIMPLE method.
- (3) Matrices assembling and coupled FSI equation solving of Eq. (2.16) using the Houbolt scheme are conducted in module ‘Solve Coupled FSI Equation’.
- (4) After solving the coupled FSI equation, the structural response is calculated, while the fluid velocity at fluid-structure interface is obtained through Eq. (2.9) in module ‘Get Structure Response’.
- (5) Then in module ‘Correct Fluid Pressure’, the fluid pressure is corrected through SOR iteration of Eq. (2.14) using the obtained

$$\left[2M/\Delta t^2 + 11C/(6\Delta t) + K \right] w^{t+\Delta t} = A_{couple_2} B_{couple} \left(A_{couple_1} w^{t+\Delta t} \right) + (5M/\Delta t^2 + 3C/\Delta t) w^t - \left[4M/\Delta t^2 + 3C/(2\Delta t) \right] w^{t-\Delta t} + \left[M/\Delta t^2 + C/(3\Delta t) \right] w^{t-2\Delta t} \quad (2.16)$$

Here, the relation between w and \dot{w} are given as $\dot{w}_{t+\Delta t} = (11w_{t+\Delta t} - 18w_t + 9w_{t-\Delta t} - 2w_{t-2\Delta t})/6\Delta t$ following the Houbolt scheme. Eq. (2.16) is a monolithic FSI equation solved in an implicit way. Within a single iteration step Δt , the fluid and structure domains are solved simultaneously. More detailed derivations, deductions, validations and convergence tests of the monolithic FSI equation can be found in Hu et al. (2016).

Fig. 1 gives the flow chart of the monolithic FSI method, explained as the following:

- (1) Module ‘Set Initial Condition’ creates meshing of the fluids and structures and sets the initial simulation parameters.

velocity at fluid-structure interface until convergence. Note that criterion $\max_{ij} |p_{ij}^{m+1} - p_{ij}^m| < 0.001\rho^f$ is applied in this FSI method, where p_{ij}^{m+1} and p_{ij}^m denote the pressures of the $(m + 1)$ th and m th iterations.

- (6) After the fluid pressure converges, real velocity of the fluid is updated using the corrected fluid pressure in module ‘Update Fluid Velocity’, while the fluid free surface is reconstructed using the VOF method.
- (7) Updating the time to the next step, the procedure goes back to module ‘Calculate Temp velocity’ again and the simulation time proceeds to the next step.

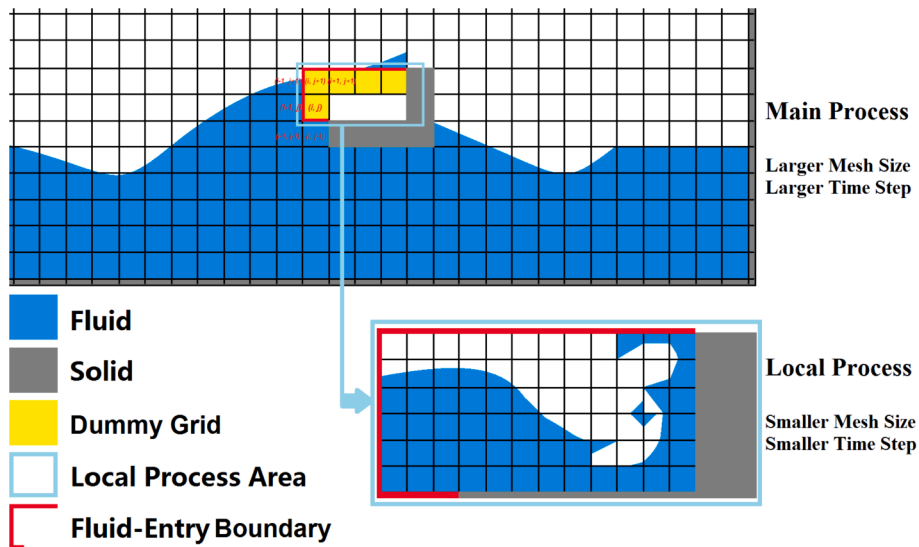


Fig. 3. Sketch of Concurrent Multi-Process Refinement method, taking a wave-induced green water event as example.

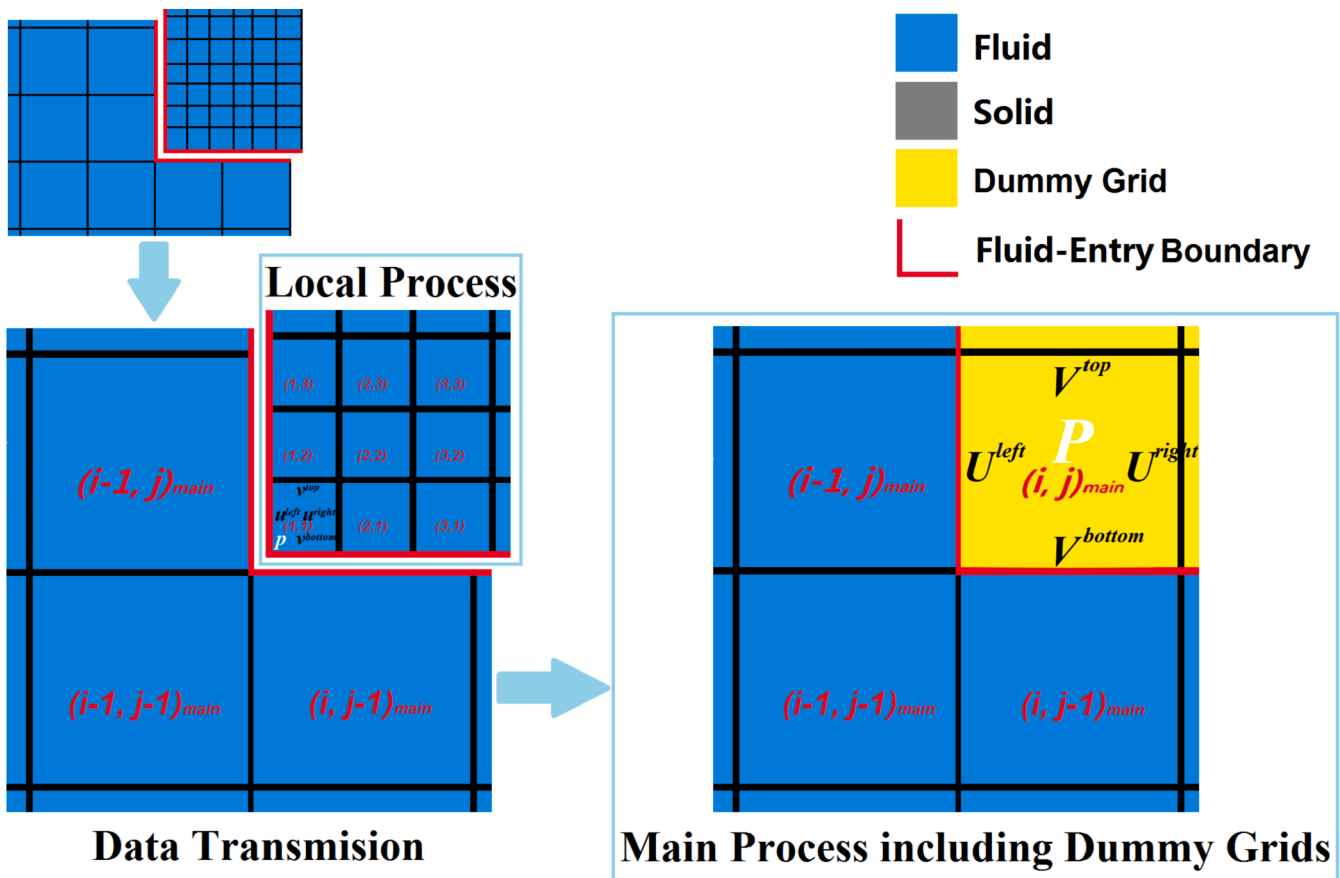


Fig. 4. Variable transmission of the fluid domain between Main Process and Local Process.

3. Concurrent Multi-Process Refinement method

3.1. Descriptions

In Section 2, the monolithic FSI method is briefly introduced, which is capable of solving various strong-coupled FSI problems. However, when encountered with realistic FSI simulation requirements such as simulations in multi-scale and with high-frequency structural vibrations,

the FSI method is faced with several problems on the efficiency and accuracy of computations, listed as follows.

Firstly, for the FSI simulation using a monolithic FSI equation, solution of the fluid domain is connected with the structure domain inseparably, which means that the simulation is conducted solving the monolithic FSI equation in the whole computational domain. Undoubtedly this would lead to extra computational costs by changing the N-S equations into the coupled FSI equations, since the conversion

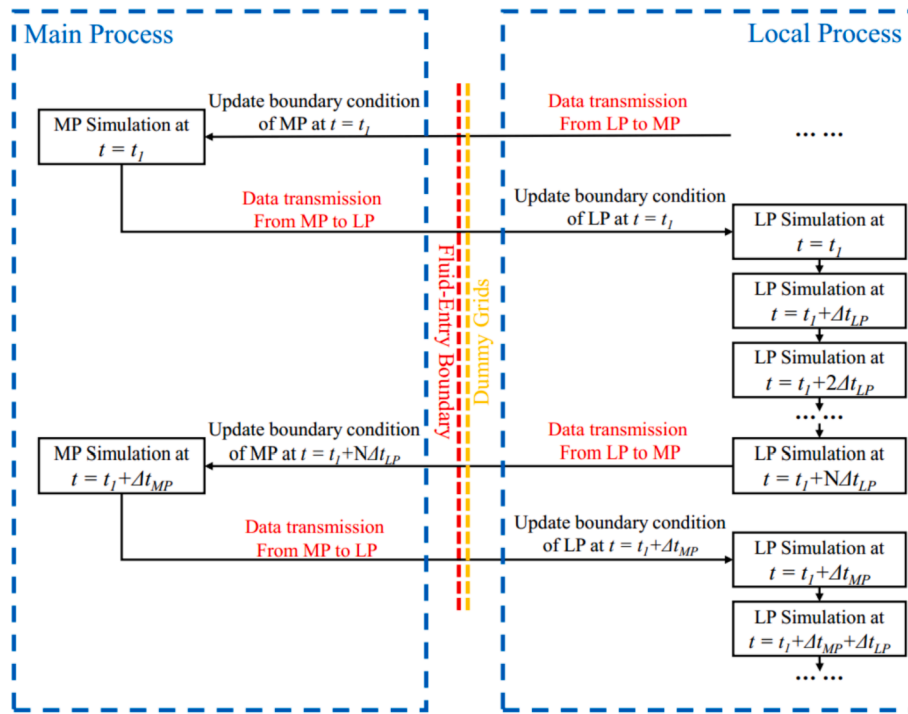


Fig. 5. Sketch of time advance in Main Process and Local Process.

matrices formed in the monolithic FSI equation Eq. (2.16) could be difficult and inefficient to solve.

Secondly, complex structures usually complicate the boundary of the fluid domain, around where grids must be refined to achieve computational accuracy. Traditional refinement method solves the large-scale matrix assembled by the governing equations in all the coarse and fine grids of the fluid domain within a single time step. However, it is known that solving a large-scale matrix is rather inefficient compared to solving several small-scale matrices, especially with ordinary computational facilities like personal computers.

Thirdly, maximum time step in the fluid domain is usually defined according to the Courant number $C_{\max} = u_{ij}(\Delta t / \Delta x)$, where u_{ij} is the fluid velocity in every grids and Δt and Δx are the corresponding time step and grid length (John and Anderson, 1995; Godderidge et al., 2006), therefore, it is seen that finer grids require smaller time step and coarser grids fit for larger time step. However, existing monolithic FSI methods assign the same time step, fixed or adaptive, to all the grids in the fluid domain regardless of the fact that only local refined grids need smaller time step, which increases the computational cost enormously.

Lastly, for FSI problems with relatively large rigidity structures (such as metal structures), time step in the structure domain would be significantly reduced compared to the time step in the fluid domain, so that the high-frequency structural vibrations could be captured accurately using high sampling frequencies. The ratio of time step between the fluid and structure domains might be up to 20 times or larger, however, for monolithic FSI equations like Eq. (2.16), it is impossible to separate the time step between the fluid and structure domains.

In this Section, a Concurrent Multi-Process Refinement method is developed, which is capable of solving the monolithic FSI problems described above. Being different from traditional refinement method, Concurrent Multi-Process Refinement method divides the computational domain into several subdomains in different processes, shown in Fig. 2. Multi-processes exist at the same time and are computed concurrently with corresponding multi-grid sizes and multi-time steps, where data of velocity and pressure variables are transmitted between two processes through Fluid-Entry Boundaries and Dummy Grids. By applying the method, efficiency and accuracy of monolithic FSI

simulations are balanced in four aspects. Firstly, the monolithic FSI equation is solved within the FSI process, while the N-S equations are solved in other processes where FSI is not included. Secondly, the fluid domain is divided into several subdomains and simulated in multi-processes with different grid sizes concurrently, which decomposes the total matrix into several smaller matrices in a single time step compared with the traditional refinement method. Thirdly, larger and smaller time steps are applied in different simulation processes, which guarantees the simulation efficiency in coarser grids and the simulation accuracy in finer grids simultaneously. Lastly, the high sampling frequency (thus small time step) requirement in the structure domain caused by the high-frequency structural vibrations is avoided in the fluid domain that is far from the FSI area and have little influence on the FSI coupling.

3.2. Numerical implementation

In order to explain the numerical implementation of Concurrent Multi-Process Refinement method developed in this paper, a specific illustration of wave-structure interaction is given. In Fig. 3, the interaction problem is divided into two processes, where generation and propagation of the wave are simulated in Main Process with a larger grid size and time step, and the interaction between wave and structure are simulated in Local Process with a smaller grid size and time step.

In Concurrent Multi-Process Refinement method, the data between Main Process and Local Process are linked and transmitted through the Fluid-Entry Boundary which is similar to the wave-making boundary (velocity inlet) in numerical implementation of wave generation, shown in Fig. 3 as the red solid lines. Dummy Grids are introduced in Main Process, shown as the yellow-colored grids in Fig. 3. As its literal meaning, Dummy Grids are 'virtual' grids, acting as virtual boundary of the fluid domain in Main Process. Fluid-Entry Boundary and Dummy Grids are the bridge of data transmissions, through which relations of variables of fluid velocity components and pressure between Main Process and Local Process are built bi-directionally. In particular, Dummy Grids act as the boundary condition for Main Process, while the column grids on Fluid-Entry Boundary within Dummy Grids act as the boundary condition for Local Process.

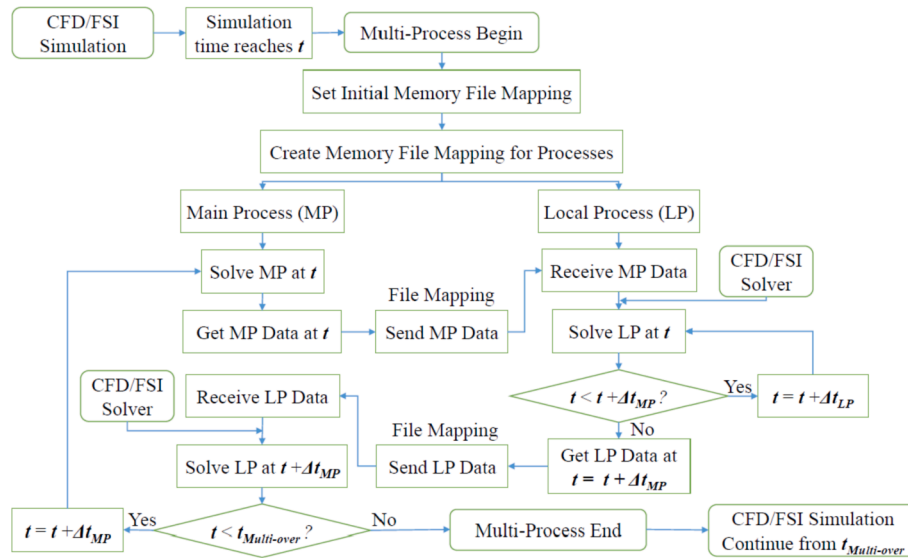


Fig. 6. Flow chart of Concurrent Multi-Process Refinement method applied in FSI simulations.

The data transmissions of variables between Main Process and Local Process are illustrated in Fig. 4. In Main Process, assuming the fluid velocity on the right, left, top and bottom boundary of Dummy Grid $(i, j)_{main}$ to be $U_{(i,j)_{main}}^{right}$, $U_{(i,j)_{main}}^{left}$, $V_{(i,j)_{main}}^{top}$ and $V_{(i,j)_{main}}^{bottom}$, while the fluid pressure at center of the grid to be $P_{(i,j)_{main}}$. In Local Process, assuming the fluid velocity on the right and top boundary of grid $(i, j)_{local}$ to be $u_{(i,j)_{local}}^{right}$, $u_{(i,j)_{local}}^{left}$, $v_{(i,j)_{local}}^{top}$ and $v_{(i,j)_{local}}^{bottom}$, while the fluid pressure at center of the grid to be p_{ij} .

On one hand, the simulation data transmit from Main Process into Local Process as:

$$u_{(i,j)_{local}}^{right} = U_{(i,j)_{main}}^{left} \cdot \frac{N_h - i}{N_h} + U_{(i,j)_{main}}^{right} \cdot \frac{i}{N_h} \quad (3.1)$$

$$u_{(i,j)_{local}}^{left} = U_{(i,j)_{main}}^{left} \cdot \frac{N_h - (i - 1)}{N_h} + U_{(i,j)_{main}}^{right} \cdot \frac{(i - 1)}{N_h} \quad (3.2)$$

$$v_{(i,j)_{local}}^{top} = V_{(i,j)_{main}}^{bottom} \cdot \frac{N_v - j}{N_v} + V_{(i,j)_{main}}^{top} \cdot \frac{j}{N_v} \quad (3.3)$$

$$v_{(i,j)_{local}}^{bottom} = V_{(i,j)_{main}}^{bottom} \cdot \frac{N_v - (j - 1)}{N_v} + V_{(i,j)_{main}}^{top} \cdot \frac{(j - 1)}{N_v} \quad (3.4)$$

$$p_{(i,j)_{local}} = P_{(i,j)_{main}} + \rho^f g \frac{N_v - (2j - 1)}{2} \Delta y_{local} \quad (3.5)$$

On the other hand, the simulation data transmit from Local Process into Main Process as:

$$U_{(i,j)_{main}}^{right} = \frac{2}{N_h + 1} \sum_{i=1}^{N_h} \left(u_{(i,j)_{local}}^{right} \cdot \frac{i}{N_h} \right) \quad (3.6)$$

$$U_{(i,j)_{main}}^{left} = \frac{2}{N_h + 1} \sum_{i=1}^{N_h} \left(u_{(i,j)_{local}}^{left} \cdot \frac{N_h - (i - 1)}{N_h} \right) \quad (3.7)$$

$$V_{(i,j)_{main}}^{top} = \frac{2}{N_v + 1} \sum_{j=1}^{N_v} \left(v_{(i,j)_{local}}^{top} \cdot \frac{j}{N_v} \right) \quad (3.8)$$

$$V_{(i,j)_{main}}^{bottom} = \frac{2}{N_v + 1} \sum_{j=1}^{N_v} \left(v_{(i,j)_{local}}^{bottom} \cdot \frac{N_v - (j - 1)}{N_v} \right) \quad (3.9)$$

$$P_{(i,j)_{main}} = \frac{1}{N_h N_v} \sum_{i=1}^{N_h} \sum_{j=1}^{N_v} p_{(i,j)_{local}} \quad (3.10)$$

Here, $N_h = \Delta x_{main} / \Delta x_{local}$ and $N_v = \Delta y_{main} / \Delta y_{local}$ are the horizontal and vertical ratio of the mesh size in Main Process against the one in Local Process, in which Δx_{main} and Δy_{main} denote the grid length in horizontal and vertical directions in Main Process; Δx_{local} and Δy_{local} denote the grid length in horizontal and vertical directions in Local Process.

Once the data transmission is completed from one process to the other, the transmitted values update the variables in Dummy Grids at Fluid-Entry Boundary. When data are transmitted from Local Process to Main Process, variables $(U_{(i,j)_{main}}^{right}, U_{(i,j)_{main}}^{left}, V_{(i,j)_{main}}^{top}, V_{(i,j)_{main}}^{bottom}, P_{(i,j)_{main}})$ are updated by $(u_{(i,j)_{local}}^{right}, u_{(i,j)_{local}}^{left}, v_{(i,j)_{local}}^{top}, v_{(i,j)_{local}}^{bottom}, p_{(i,j)_{local}})$ through Eq. (3.6)–(3.10). Then variables such as velocity and pressure in Main Process are calculated using the updated new boundary condition of Dummy Grids. When data are transmitted from Main Process to Local Process, $(u_{(i,j)_{local}}^{right}, u_{(i,j)_{local}}^{left}, v_{(i,j)_{local}}^{top}, v_{(i,j)_{local}}^{bottom}, p_{(i,j)_{local}})$ are updated by $(U_{(i,j)_{main}}^{right}, U_{(i,j)_{main}}^{left}, V_{(i,j)_{main}}^{top}, V_{(i,j)_{main}}^{bottom}, P_{(i,j)_{main}})$ through Eq. (3.1)–(3.5). Then velocity and pressure in Local Process are calculated using the new boundary condition of the column grids on Fluid-Entry Boundary within Dummy Grids.

The descriptions above explains the data transmission between multi-processes in ‘one time step’. Note that ‘one time step’ here denotes the last time step in Local Process when data are transmitted from Local Process to Main Process, or the last time step in Main Process when data are transmitted from Main Process to Local Process. To better explain the time advance strategy, Fig. 5 gives the sketch of the time relation between Main Process (MP) and Local Process (LP) temporally. Firstly, assuming the computational domain at $t = t_1$ is already known, while the selected time steps for Main Process and Local Process are Δt_{MP} and Δt_{LP} respectively. Also assuming the relation of $\Delta t_{MP} = N \Delta t_{LP}$ exist, where N is the ratio between time steps. Through Fluid-Entry Boundary and Dummy Grids, data from Main Process at $t = t_1$ are transmitted to Local Process and the boundary condition of Local Process is updated. Secondly, simulations from $t = t_1$ to $t = t_1 + N \Delta t_{LP}$ are carried out in Local Process, after which data from Local Process at $t = t_1 + N \Delta t_{LP}$ are transmitted to Main Process and the boundary condition of Main Process is updated. Note that relation $t = t_1 + N \Delta t_{LP} = t_1 + \Delta t_{MP}$ exist. Thirdly, the simulation at $t = t_1 + \Delta t_{MP}$ is conducted, which means that the simulation of Main Process proceeds to the next time step. This time

advance relation starts and ends at the certain time when the multi-process refinement is applied and canceled. Note that the data exchange between Main Process and Local Process at Fluid-Entry Boundary and Dummy Grids, which are within the pure fluid domain rather than at the fluid-structure interface. Moreover, the resolution of the fluid and structure parts are still solved as one entity in Local Process. Therefore, Concurrent Multi-Process Refinement method do not change the fact that the FSI method is a monolithic method rather than a partitioned method, the latter of which solve the fluid and structure parts in different entities using staggered approach or non-staggered sub-iteration/synchronization techniques (Felippa et al., 2001).

3.3. Algorithm procedure

The FSI method in Section 2 and Concurrent Multi-Process Refinement method is compiled using Visual Basic language and operated in a computational station which consists of an 8-core 3.60 GHz CPU and a 12.0 GB RAM. Data transmission of Concurrent Multi-Process Refinement method is based on the File Mapping approach provided by Visual Basic, which creates mapping relations from disk files to computer memory. Using this approach, the link between different processes can be built by transmitting data through visiting memory rather than disk files, leading to an increase of the data access speed among processes. When Concurrent Multi-Process Refinement method operates, it first creates the file mapping of each process, and then built the links of data transmission between processes by directly visiting memory. The received data in each process update the boundary conditions for simulations, while the data obtained through simulations are further saved in memory for the next data transmission.

Fig. 6 gives the flow chart of Concurrent Multi-Process Refinement method applied in the monolithic FSI method SBMIM, from which the programming procedure of the algorithm is illustrated. As can be seen, procedure Concurrent Multi-Process Refinement method is composed of the following steps (1)–(9). Note that Fig. 6 and steps (1)–(9) takes a two-process simulation as example, however, Concurrent Multi-Process Refinement method is able to operate with more than two processes.

- (1) The CFD/FSI simulation in one process continues until simulation time reaches time t when concurrent multi-process simulations are set to begin.
- (2) At time t , multi-process simulations begin with ‘Set Initial Memory File Mapping’ module, which initializes the names and parameters of file mappings and disk files for the variables and mesh grids in different processes.
- (3) ‘Create Memory File Mapping for Processes’ module creates the file mappings between disk files and the computer memory for processes that need to be linked for data transmissions. In this module, different mapping addresses between each two multi-processes are created and assigned in memory respectively, where data between two multi-processes can be visited and transmitted.
- (4) When file mappings of the multi-processes are built, the CFD/FSI simulation can be carried out in multi-processes using the method in Section 2. Taking a two-process division as example, the simulation is divided into one Main Process (MP) with time step Δt_{MP} and one Local Process (LP) with time step Δt_{LP} . Note that $\Delta t_{MP} > \Delta t_{LP}$.
- (5) Assuming the simulation at time t in Main Process has already been finished, data for transmission at this time are obtained from the simulation results of Main Process in ‘Get MP Data at t ’ module and sent to the computer memory in ‘Send MP Data’ module through the file mapping created before.
- (6) Local Process accesses the data from Main Process in ‘Receive MP Data’ module by visiting the memory and is solved with time step Δt_{LP} . The simulation of Local Process is conducted until the simulation time reaches $t + \Delta t_{MP}$ when the simulation of Main

Process should be continued to update the boundary conditions for Local Process.

- (7) Data of variables of Local Process at $t + \Delta t_{MP}$ are obtained in ‘Get LP Data at $t + \Delta t_{MP}$ ’ module and sent to Main Process in ‘Send LP Data’ module through file mapping.
- (8) Received by Main Process in ‘Receive LP Data’ module, data from Local Process updates the boundary conditions for Main Process. Then the simulation of Main Process is conducted with time step Δt_{MP} until the simulation time reaches $t + 2\Delta t_{MP}$.
- (9) Looping the steps from (5)–(8) until the simulation time reaches the total simulation time $t_{Multi-over}$ set for multi-process simulations, the multi-process simulation is over and the CFD/FSI in one process continues from time $t_{Multi-over}$.

3.4. Advantages and limitations

Advantages of Concurrent Multi-Process Refinement method are analyzed first. As we know, FSI methods can be divided into two categories considering the coupling manners, which are the partitioned FSI methods and monolithic FSI methods. Partitioned FSI methods solve the fluid and structure domains respectively and iteratively. In each time step, the fluid solver predicts the position, velocity and pressure of all grids or particles on the fluid-structure interface within the fluid domain. Then the fluid force is acted on the structure domain to calculate the deformation and velocity of the structure, while the updated variables of the deformable structure is applied back to the fluid domain to correct the fluid velocity and pressure until convergence. As a result, the total iteration number would be the iteration number of fluid (denoted as M_1) multiply the iteration number of structure (denoted as N_1), that is $M_1 \times N_1$. On another aspect, monolithic FSI methods such as SBMIM establish a monolithic FSI equation using the continuity relation between the fluid and structure domains. In each time step, variables of the fluid and structure domains such as the velocity and pressure of fluid grids, and deformation and velocity of structure elements are solved using the monolithic FSI equation at the same time. As a result, the total iteration number would be the iteration number of solving the monolithic FSI equation. Since SBMIM constructs the monolithic FSI equation through the pressure Poisson equation of the fluid using mobile solid boundaries (Hu et al., 2016), the total iteration number would be the iteration number of the fluid (denoted as M_2). Usually, a relation of $M_2 < M_1 \times N_1$ is expected since M_1 and M_2 are close in value, and thus the monolithic FSI method in this paper is relatively computational inexpensive compared to the partitioned FSI methods.

The monolithic FSI equation usually complicates the governing equations, making it more difficult to get the solution compared with pure-CFD simulations. In addition, the monolithic FSI equation requires a unified time step for both the fluid and structure domains, although the time step of the fluid domain according to the Courant number criterion can be much larger than the time step of the structure domain when a high sampling frequency is requirement for high-frequency structural vibrations. To deal with these two problems, Concurrent Multi-Process Refinement method divides the large-scale computational domain into processes of FSI simulations and pure-CFD simulations. The dimension of the monolithic FSI equation is reduced by localizing the FSI area, while the unnecessary unified time step is avoided by different time steps. To solve the monolithic FSI equation, traditional refinement (shown in Fig. 2-a) requires a simulation time of $T_2 \times M_2$, where T_2 is the time step number and M_2 is the iteration number in one time step. Multi-process refinement (shown in Fig. 2-b) requires a simulation time of $(T_2/R_{ML}) \times M_M + T_2 \times M_L$, where M_M and M_L are the iteration number of Main Process and Local Process in one time step, and R_{ML} is the ratio of time step of Main Process against time step of Local Process. Since $M_2 > M_M + M_L$ is expected due to the larger application area of the monolithic FSI equation using traditional refinement, it is easy to found that $T_2 \times M_2 > (T_2/R_{ML}) \times M_M + T_2 \times M_L$, indicating that Concurrent Multi-Process Refinement method can further lower the computation

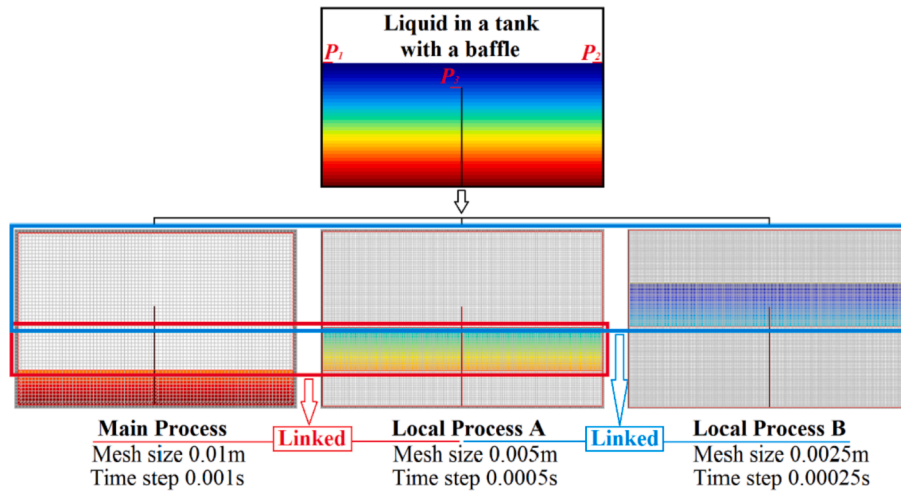


Fig. 7. The liquid sloshing in a tank with a baffle (Top Panel) and the division of different processes (Bottom Panel).

Table 1

Grid sizes and time steps in the liquid sloshing case.

Simulation Case	Grid size	Time step	Computational cost
Coarse grid	0.0100 m	0.00100s	1 h
Medium grid	0.0050 m	0.00050s	7 h
Fine grid	0.0025 m	0.00025s	66 h
Multi-process	Main Process	0.0100 m	0.00100s
	Local Process A	0.0050 m	0.00050s
	Local Process B	0.0025 m	0.00025s

cost in monolithic FSI methods compared to the traditional refinement method.

There are also some limitations of Concurrent Multi-Process Refinement method. For simulations containing FSI and elastic responses of structures, when the computation domain is divided into Main Process and Local Process, the monolithic FSI equation is only

solved in Local Process, while pure-CFD simulation is conducted in Main Process. As a result, FSI effects, mainly the added mass effects, are actually not included in Main Process, narrowing the area actually influenced by FSI. Therefore, it should be noted that the area selection of Local Process should be careful, so that the FSI effects would not be under-estimated. For simulations containing FSI and elastic responses of structures, it is recommended that a refinement study on area selection should be carried out first to determine the Local Process area near the elastic structures and the Main Process area far from the elastic structures. In this paper, a detailed refinement study on Local Process selection can be found in Section 4.2, in which an error estimation is carried out. Also, compared with massive parallel FSI simulations using super computers, Concurrent Multi-Process Refinement method might lose its advantage in efficiency since this method is designed for low-cost computational facilities like ordinary personal computers.

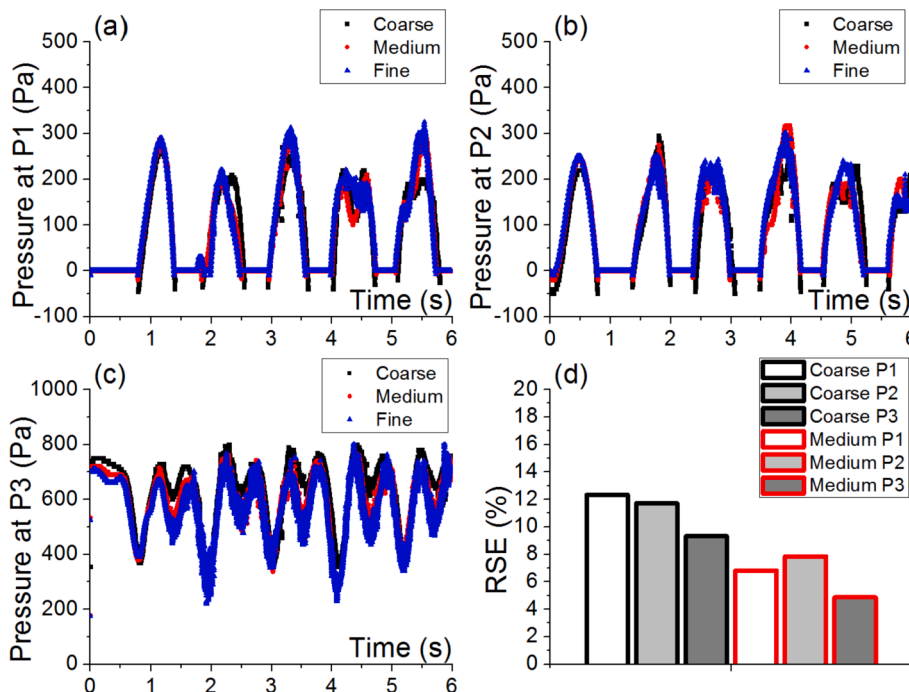


Fig. 8. Pressure time histories of pressure for the coarse, medium and fine grids at pressure monitors (a) P₁, (b) P₂, (c) P₃; and (d) the relative standard error of the coarse and medium grids.

Table 2
Error estimation on coarse, medium and fine grids using GCI.

Location	Mean Pressure/Pa			p	GCI ₂₁	GCI ₃₂
	Fine	Medium	Coarse			
P ₁	86.3	85.4	83.4	1.15	1.1%	2.4%
P ₂	94.5	93.3	91.0	0.94	1.7%	3.4%
P ₃	572.8	590.5	632.1	1.23	2.9%	6.5%

4. Refinement study

In this section, two cases of refinement study are introduced using Concurrent Multi-Process Refinement method applied in the monolithic FSI method, including the liquid sloshing in a baffled tank and the dam breaking flow slamming an elastic vertical wall. The liquid sloshing case shows the performance of Concurrent Multi-Process Refinement method in CFD simulation with nonlinear free surface evolutions, and gives an error estimation on different refinements including coarse, medium, fine and multi-process grids. The dam breaking case compares the results by present methods and by previous literatures, and gives an error estimation on refinements with different Local Process areas.

4.1. Liquid sloshing in a baffled tank

The liquid sloshing in a baffled tank is one typical CFD case which has been widely investigated and considered suitable for the refinement study. The top panel of Fig. 7 gives the illustration of the liquid sloshing in a tank with a baffle, which is designed similar to the one in Jung et al. (2012). The tank is 0.8 m in length and 0.5 m in height, while the liquid (which is water) in the tank is 0.35 m in depth. A fixed rigid 0.28 m-long baffle is clamped at the middle of the tank bottom; three pressure gauges are installed at the left (P₁), right (P₂) wall of the tank and left-top (P₃) of the baffle to monitor fluid pressures. The tank is under pure-surge motion, defined by the sinusoidal function of:

$$Xs = As \sin(\omega t) \tag{4.1}$$

where Xs is the surge motion transversally. As and ω are the amplitude and frequency of the surge motion, which are fixed as As = 0.02m and ω = 5.82rad/s respectively. Physical properties within the fluid domain are chosen as: fluid density 1000 kg/m³, fluid kinematical viscosity 0.000001145 m²/s, air pressure 101263.4Pa, acceleration of gravity 9.81 m/s².

Following the Courant number criterion, three groups of grid sizes and time steps are adopted to give a grid-independence test, which are the coarse, medium and fine grids, shown in Table 1. In addition, a multi-process grid using Concurrent Multi-Process Refinement method is applied to compare with the coarse, medium and fine grids, in which the three processes are named as Main Process, Local Process A and Local Process B, shown in the bottom panel of Fig. 7. The total simulation time for the coarse, medium, fine and multi-process grids are 6s, including five whole sloshing periods.

Firstly, a grid-independence test on the liquid sloshing are conducted with the coarse, medium and fine grids, which cost 1 h, 7 h and 66 h of computation respectively. The time histories at pressure monitors P₁, P₂ and P₃ are shown in Fig. 8-a, Fig. 8-b and Fig. 8-c, indicating that a rather satisfactory agreement among the three simulation cases. However, using the relative standard error (RSE), deviations of the pressure results with coarse and medium grids are obtained based on the pressure results with the fine grid, given in Fig. 8-d. It is seen that the RSEs of the coarse grid are 12.3%, 11.7% and 9.3% at P₁, P₂ and P₃, while the RSEs of the medium grid are 6.8%, 7.8% and 4.8% at P₁, P₂ and P₃. By halving the grid size and time step from coarse to medium grid, the relative standard error is reduced by more than 42% averagely, but the computational cost is increased by about seven times.

It was stated that a recommended method for grid refinement study and error estimation is called the Grid Convergence Index (GCI) method (Celik et al., 2008), which was based on the Richardson Extrapolation (Richardson, 1911). GCI is a measure of the percentage of how far the

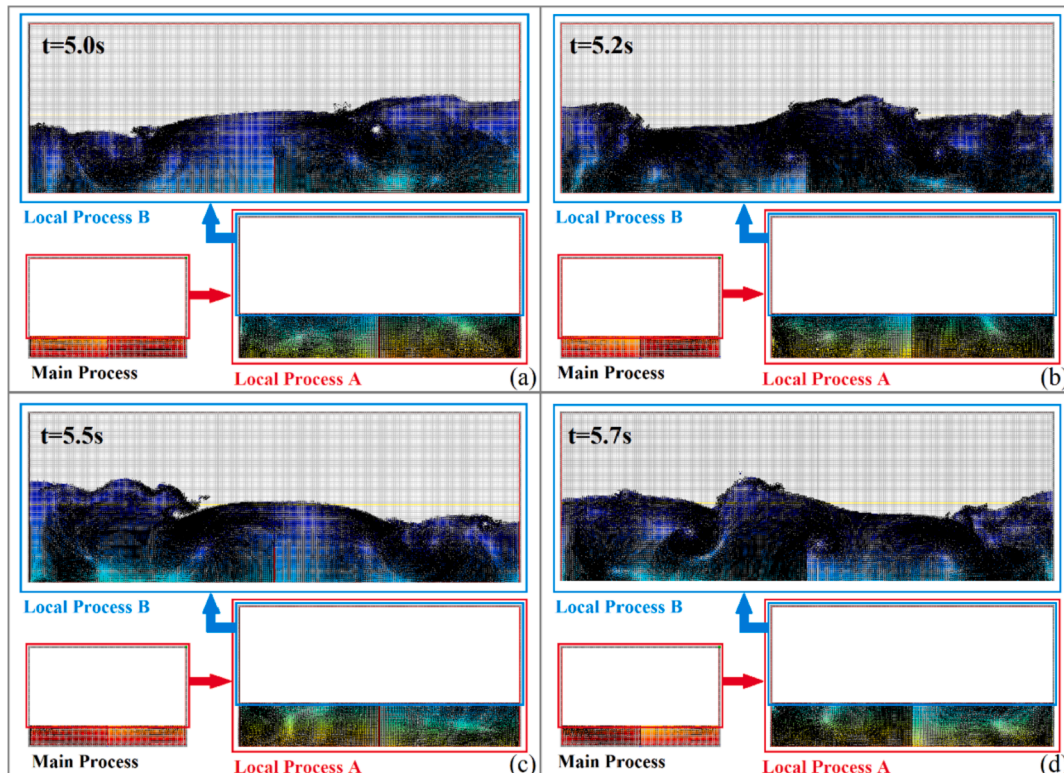


Fig 9. Snapshots of the liquid sloshing in Main Process, Local Process A and Local Process B using Concurrent Multi-Process Refinement method.

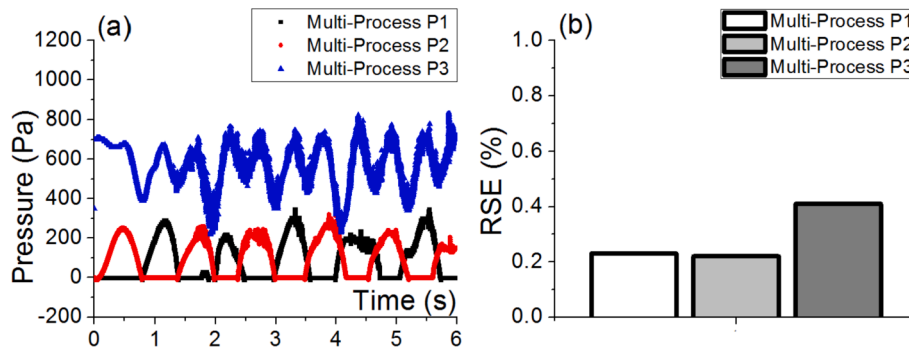


Fig. 10. Pressure time histories for multi-process grid at pressure monitors P₁, P₂ and P₃ (Left Panel); and the relative standard error of multi-process grid against fine grid (Right Panel).

Table 3
Error estimation on medium, multi-process and fine grids using GCI.

Location	Mean Pressure/Pa			p	GCI ₂₁	GCI ₃₂
	Fine	Multi-Process	Medium			
P ₁	86.3	86.2	85.4	6.42	<0.5%	1.6%
P ₂	94.5	94.6	93.3	7.75	<0.5%	1.4%
P ₃	572.8	573.0	590.5	13.63	<0.5%	4.0%

Table 4
Grid sizes and time steps in the dam breaking case.

Simulation Case		Grid size	Time step	Computational cost
Coarse grid		0.008 m	0.0008s	0.25 h
Fine grid		0.004 m	0.0004s	0.83 h
Multi-process	Main Process	0.008 m	0.0008s	0.52 h
	Local Process	0.004 m	0.0004s	
Previous literature		Particle distance	Maximum time step	Computational cost
Sun et al. (2015)		0.004 m	0.0010s	1.00 h
Zhang and Wan (2018)		0.004 m	0.0005s	Not reported

computed value is away from the asymptotic numerical value, and has been evaluated over several hundred cases. Procedures and formulas of the GCI method can be found in many previous papers (Roache, 2003; Celik et al., 2008; Park et al., 2015; etc.), and thus they are not listed here.

Table 2 shows the mean values of the key variable, which is pressure, obtained from the fine grid (subscript 1), medium grid (subscript 2) and coarse grid (subscript 3) solutions, and the results of corresponding GCIs. Note that GCI₂₁ means the GCI of medium grid against fine grid, while GCI₃₂ means the GCI of coarse grid against medium grid. It is seen that there is a reduction in GCIs with successive grid refinement, indicating the solution is reaching towards a grid-independent result. In addition, GCI₃₂ at pressure monitor P₃ is much larger than the ones at P₁ and P₂, which means that medium grid performs well at P₁ and P₂, but leads to a relatively larger error at P₃. Thus to obtain a convinced pressure value at P₃, a fine grid might be necessary.

After conducting the grid-independence test, the simulation of liquid sloshing using Concurrent Multi-Process Refinement method is carried out. Fig. 9 illustrates the snapshots of the liquid sloshing in the last surge period of the tank using multi-process grid, in which the grid size reduces from the bottom to the free surface of the tank in three divided-

linked processes. It is seen that within the area in Local Process B, the fine grid shows good performance in vortex and free surface evolutions. The vortices induced by the baffle are still clear in direction and size although the baffle is relatively long, besides, new-small vortices along with the rolling and breaking of the free surface can be captured which are not shown in Jung et al. (2012). In fact, the vortex and free surface evolutions in Jung et al. (2012) were relatively coarse and simple due to the reason of using a relatively coarse grid compared to the multi-process grid in this paper, which still showed good agreement with the experimental measurement and existing numerical results. However, the vortex in the finer grid and the violent rolling and breaking of the free surface surely have an important influence on the loads acting on the wall and baffle of the tank, for instance the comparison of pressures in Fig. 8 shows that the finer grid is not only more precise according to the RSE and GCI but also on the depth of the amplitude (peak and trough) in one period of sloshing, which are induced by the vortex and free surface elevations.

The pressure time histories of the multi-process grid at pressure monitors P₁, P₂ and P₃ and the RSEs of the multi-process grid against the fine grid are given in Fig. 10. By comparing the pressure histories from the multi-process grid in Fig. 10-a and the fine grid in Fig. 8, it is seen that the multi-process grid shows good agreements with the fine grid on pressures. The RSEs of the multi-process grid against the fine grid at P₁, P₂ and P₃ are merely 0.2%, 0.2% and 0.4% respectively, indicating that the relative standard error between multi-process grid using Concurrent Multi-Process Refinement method and the fine grid in the whole simulation area is small enough to be neglected. In the meanwhile, among the fine grid (subscript 1), multi-process grid (subscript 2) and medium grid (subscript 3), GCIs are calculated in Table 3, from which it is seen that GCIs of multi-process grid against fine grid are all smaller than 0.5%. Therefore, from view of both the vortex and free surface evolutions, and the pressure time histories, Concurrent Multi-Process Refinement method performs satisfactorily as a refinement method. Additionally, shown in Table 1, applying the multi-process grid reduced the computational cost by more than half compared to the fine grid, which proves that Concurrent Multi-Process Refinement method balanced the accuracy and efficiency at the same time. It should be clarified that when studying the sloshing loads on the side walls of the liquid tank and the sloshing loads on the vertical baffle are not focused, a medium grid is enough for the accuracy of simulation. However, when attention is paid on the sloshing loads on the vertical baffle, especially the loads near the upper end of the baffle, a fine grid or multi-process grid using Concurrent Multi-Process Refinement method should be applied.

4.2. Dam breaking flow slamming a vertical wall

The dam breaking flow slamming an elastic vertical wall is widely used to validate FSI methods since the violent free surface movement and strong impact are involved. The case is designed similar to the ones

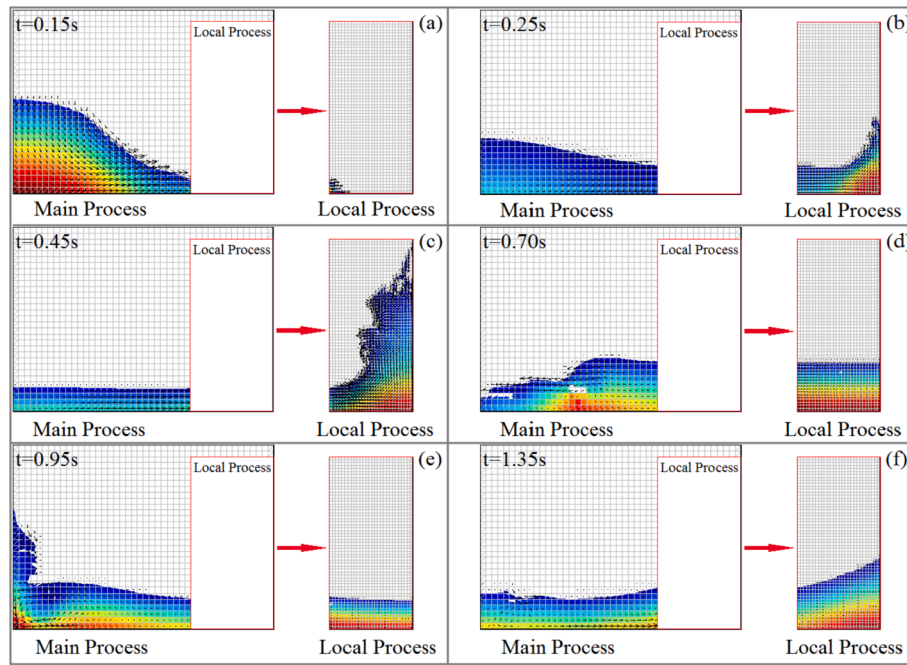


Fig. 11. Snapshots of dam breaking flow slamming a vertical wall in Main Process and Local Process using Concurrent Multi-Process Refinement method.

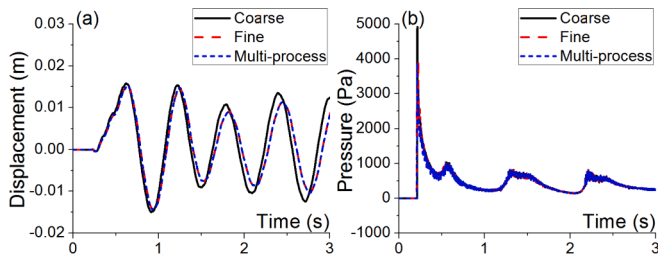


Fig. 12. Displacements at the free end and pressures at PG with different grid systems.

by Sun et al. (2015) and Zhang and Wan (2018), who used different MPS-FEM methods. A 0.1 m × 0.2 m water dam breaks and slams an elastic vertical wall 0.352 m away from it. The 0.352 m-high vertical wall is fixed at the lower end and free at the upper end. A pressure gauge PG is placed on the wall, 0.02 m from its lower end. Physical properties are chosen as: fluid density 1000 kg/m³, fluid kinematical viscosity 0.00001145 m²/s, air pressure 101263.4Pa, acceleration of gravity 9.81 m/s², elastic modulus of wall 0.2 GPa, Poisson's ratio 0.3, wall density 7860 kg/m³, wall thickness 0.006 m.

In the fluid domain, three groups of grid sizes are applied, which are the coarse, fine and multi-process grids shown in Table 4, while in the structure domain, the elastic vertical wall is discretized into 61 elements. Note that the fine grid case gives a fluid grid number of 1250, which is the same with the number of fluid particles used by Sun et al. (2015). The whole simulation time is 10s, and time step is chosen as 0.0001s, small enough to capture the high-frequency vibration of the elastic vertical wall and to guarantee the Maximum Courant number < 1 for unknown fluid fields (John and Anderson, 1995).

From the computation cost of the coarse, fine and multi-process grids in Table 4, it is seen that the fine grid case takes about 0.83 h of computational cost, which is over 3 times of the computational cost of the coarse grid case due to the smaller time step and larger number of grids. Compared to the CPU time of the simulation by Sun et al. (2015) which was 1 h, the computational cost of the fine grid case in this paper is smaller, since a monolithic FSI method is used in present study, while Sun et al. (2015) applied a partitioned MPS-FEM method. As explained in Section 3.4, the partitioned method is usually more computational expensive since iterations exist in both the fluid and structure domains. By using Concurrent Multi-Process Refinement method, the simulation time is further reduced from 0.83 h to about 0.52 h, indicating that Concurrent Multi-Process Refinement method is able to further improve

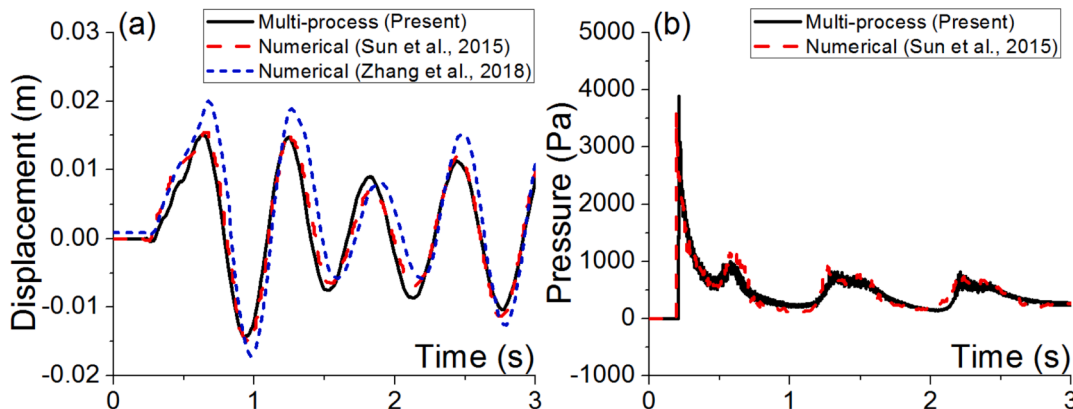


Fig. 13. Comparisons of displacements at the free end and pressures at PG.

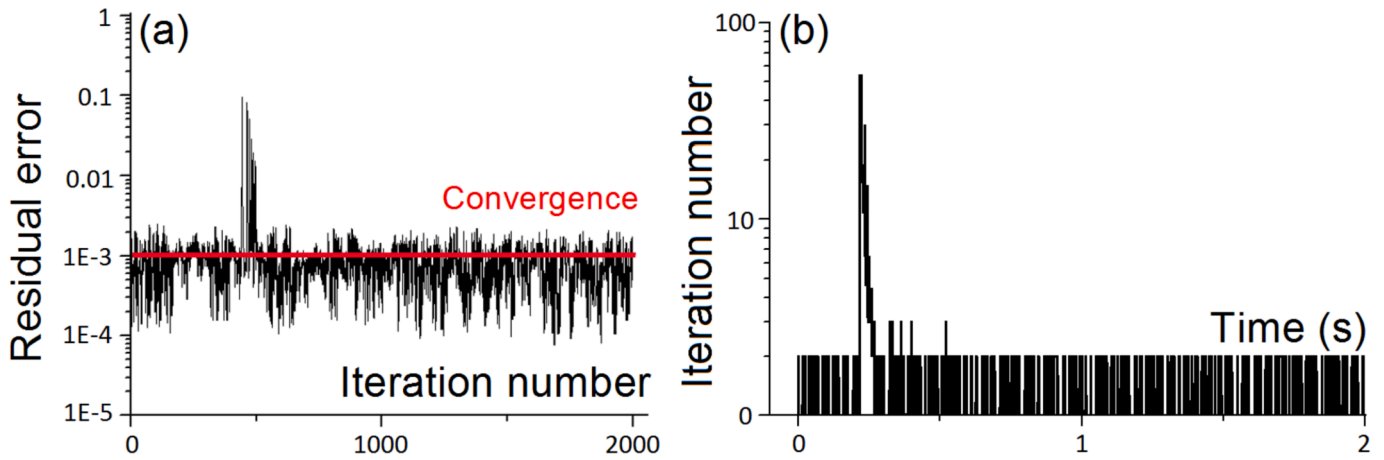


Fig. 14. Residual error and iteration number of the multi-process simulation case.

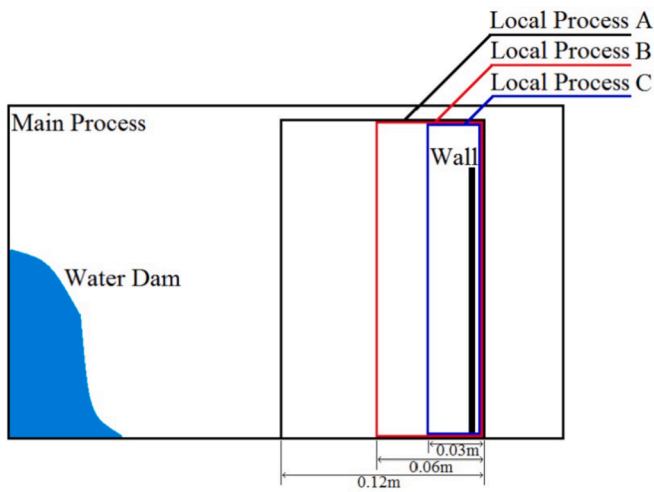


Fig. 15. Snapshot of three groups of Multi-Process refinement.

the efficiency of FSI simulation by localizing the FSI area and applying different time steps in multi-processes.

Fig. 11 illustrates the snapshots of the dam breaking flow slamming event, from which it is seen that the computational domain is divided into Main Process and Local Process using Concurrent Multi-Process Refinement method. The area near the vertical wall is refined in Local Process to guarantee the accuracy of the FSI simulation, while the area far from the vertical wall is with a coarse grid system to accelerate the computation. As expected, Local Process gives good performance in the FSI area near the vertical wall, such as the water impinging, climbing,

rolling, breaking and falling, while Main Process controls the flow behavior that is relatively far from the vertical wall without considering FSI.

Fig. 12 gives the comparison of displacements at the wall free end and pressures at PG among the coarse, fine and multi-process grids, showing that the coarse grid relatively produces larger errors both in displacement and pressure, while the results of the fine grid and multi-process grid are almost identical. In order to validate the numerical methods, displacement at the free end and pressure at PG of present results are compared with the numerical results by Sun et al. (2015) and Zhang and Wan (2018). It is seen from Fig. 13-a that the displacement of present results agrees well with the one by Sun et al. (2015) and Zhang and Wan (2018), although there are some acceptable discrepancies. From Fig. 13-b, it is observed that there is satisfactory agreement of the fluid pressures at PG between present result and the result by Sun et al. (2015), however, the pressure was not given by Zhang and Wan (2018). Therefore, from both the displacement of the vertical wall and the fluid pressure on the wall, the present FSI method and Concurrent Multi-Process Refinement method are capable of producing good results compared with the previous literatures. Additionally, by using Concurrent Multi-Process Refinement method, the computational cost can be further reduced than the original monolithic FSI method.

Fig. 14 depicts the residual error and iteration number of Local Process of the multi-process simulation case in Table 4. It is seen that at about 0.2–0.25s when initial slamming happens, the residual error and iteration number are both relatively larger than average. However, the residual error decreases quickly with the iteration number, showing a concave decreasing function during one time step as can be seen from the logarithmic coordinate of Fig. 14-a. In the meanwhile, the iteration number decreases quickly with the simulation time and is stabilized between 1 and 5 after initial slamming as shown in Fig. 14-b. Therefore,

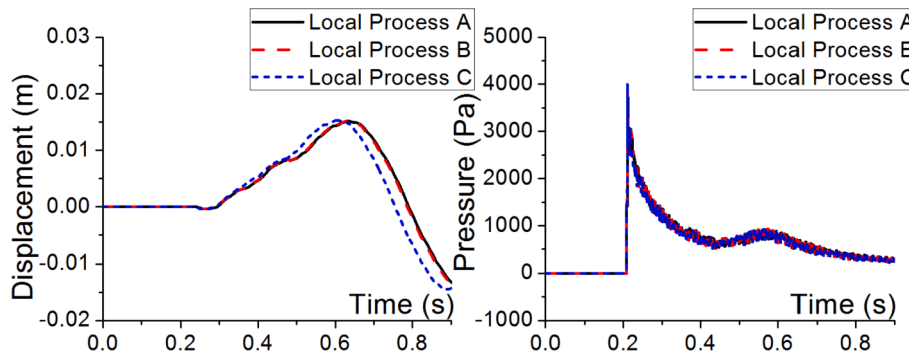


Fig. 16. Displacements at the free end and pressures at PG with different Local Process.

Table 5
Error estimation on different local processes using GCI.

Vibration frequency in the 1st half period/Hz			p	GCI ₂₁	GCI ₃₂
Local Process A	Local Process B	Local Process C			
0.988	0.995	1.034	6.40	<0.5%	2.2%
Maximum pressure at PG/Pa			p	GCI ₂₁	GCI ₃₂
Local Process A	Local Process B	Local Process C			
3887.3	3929.5	4015.1	3.59	<0.5%	3.5%

it is proven that the present FSI method (SBMIM) and Concurrent Multi-Process Refinement method give good performance on convergence.

Since one nature and purpose of Concurrent Multi-Process Refinement method is to reduce the area of localized monolithic FSI coupling in multi-scale problems, a proper choice of Local Process area becomes a key issue. In order to choose proper Local Process area, refinement study on the effect of Local Process area is carried out based on the multi-process refinement in Table 4. Three groups of Local Process selections are applied, named as Local Process A, Local Process B and Local Process C. Here, Main Process and Local Process A are designed exactly the same with Main Process and Local Process in Table 4, while Local Process B halves Local Process A and Local Process C further halves Local Process B in the horizontal direction, as shown in Fig. 15. Particularly, area lengths in the horizontal direction of Local Process A, Local Process B and Local Process C are 0.12 m, 0.06 m and 0.03 m respectively. Grid sizes and time steps of the three local processes are selected the same with the ones of Local Process in Table 4, which are 0.004 m and 0.0004s. All the other physical properties stay the same with the previous choices.

Displacements at the wall free end and pressures at PG obtained in Local Process A, Local Process B and Local Process C are shown in Fig. 16. On one aspect, it is observed that in the 1st half period of structural vibration, Local Process C gives smaller vibration period (thus higher frequency) than Local Process A and Local Process B. The reason lies in that Local Process C might be too small for the localized FSI

Table 6
Grid sizes and time steps in three different processes of green water impact.

Process	Grid size	Time step	Simulation time	Computational cost
Main Process	0.020 m	0.00200s	20s	0.8 h of CFD simulation
Local Process A	0.010 m	0.00100s	1s	0.1 h of CFD simulation
Local Process B	0.005 m	0.00005s	1s	0.9 h of FSI simulation

simulation to accurately highlight the added mass induced by the strong coupling between the fluid and structure. On the other aspect, the vibration periods obtained in Local Process A and Local Process B are quite close, indicating that Local Process B might be enough for the accurate calculation of the added mass in the localized FSI simulation.

Using the GCI method, the structural vibration frequency and maximum pressure at PG are deemed as the key variables both from the structure and fluid points of view. It should be mentioned that the structural vibration frequency here is limited within the 1st half period of the structural vibration, as the strong FSI process has already finished after water falling and free vibration dominates after the 1st half period, depicted in Fig. 11. Table 5 gives GCIs among Local Process A (subscript 1), Local Process B (subscript 2) and Local Process C (subscript 3). The result shows that the convergence conditions of both key variables are monotonic as there are reductions in the GCIs of both key variables with successive grid refinement ($GCI_{21} < GCI_{32}$), which indicates that the dependency of the simulation results on the grid size has been reduced and the solution is reaching towards the grid-independent solution. It is also shown that GCI_{21} calculated between Local Process A and Local Process B is rather small in view of both key variables, in the meanwhile, GCI_{32} calculated between Local Process B and Local Process C is relatively larger. As such, GCIs among different local processes prove the conclusion that Local Process B might be enough for the localized FSI simulation but Local Process C might be too limited for the accurate calculation of the added mass in the strong coupling between the fluid

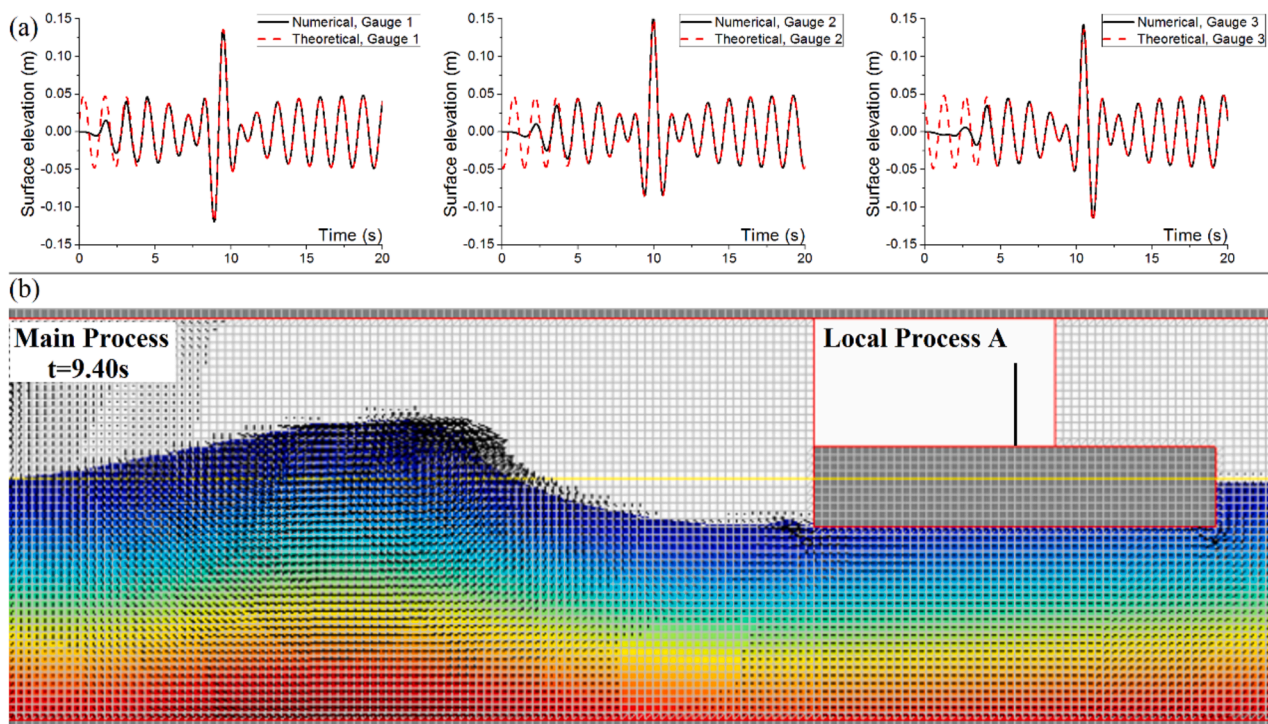


Fig. 17. Free surface elevations of generated freak wave at Gauge 1, Gauge 2 and Gauge 3 (Top Panel), and the free surface snapshot before freak wave reach the platform (Bottom Panel).

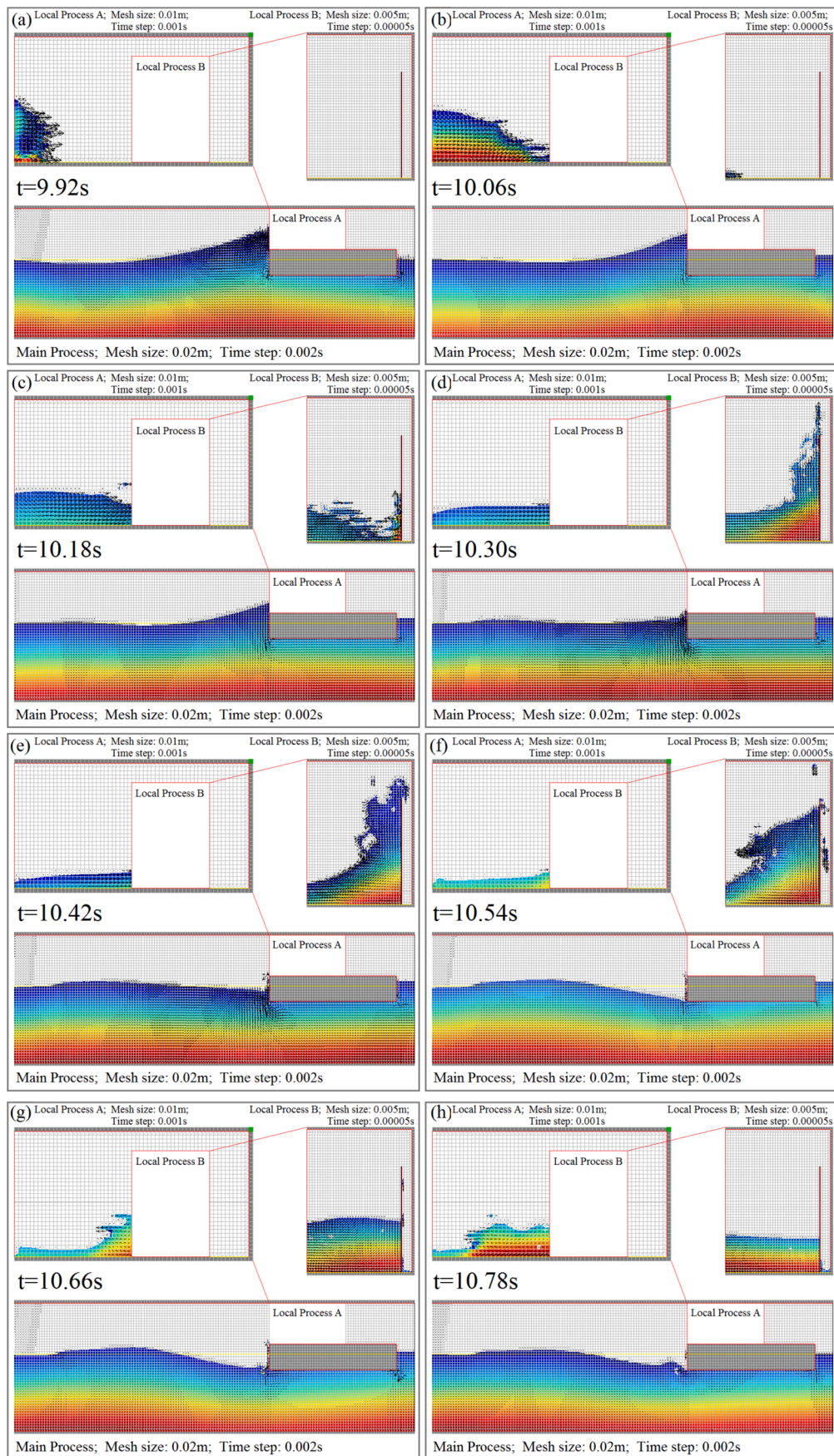


Fig. 18. Snapshots of the green water impact caused by freak wave in Main Process, Local Process A and Local Process B using Concurrent Multi-Process Refinement method.

Table 7
Comparison of computational cost.

Process	Grid size	Time step	Simulation time	Computational cost
Main Process	0.005 m	0.00050s	20s	>100 h of FSI simulation
Main Process	0.020 m	0.00200s	20s	0.8 h of CFD simulation
Local Process A	0.005 m	0.00005s	1s	2.3 h of FSI simulation
Main Process	0.020 m	0.00200s	20s	0.8 h of CFD simulation
Local Process A	0.010 m	0.00100s	1s	0.1 h of CFD simulation
Local Process B	0.005 m	0.00005s	1s	0.9 h of FSI simulation

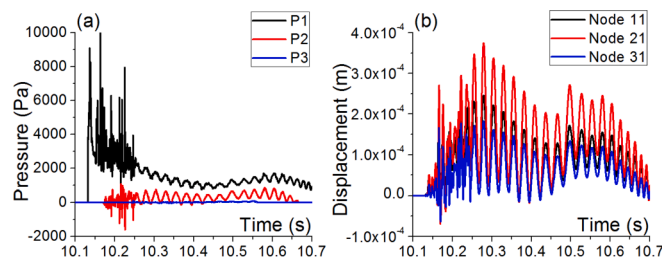


Fig. 19. Pressure time histories (Left Panel) and nodal displacements (Right Panel).

Table 8
Grid sizes and time steps in four different processes.

Process	Grid size	Time step	Simulation time	Computational cost
Main Process	0.020 m	0.002000s	20s	0.8 h of CFD simulation
Local Process A	0.0100 m	0.001000s	1s	0.1 h of CFD simulation
Local Process B	0.0050 m	0.000500s	1s	0.2 h of CFD simulation
Local Process C	0.0025 m	0.000025s	1s	1.1 h of FSI simulation

and structure. It is suggested by the authors that Local Process selection is suitable when GCI of key variables are smaller than 1%, so that the strong coupling between the fluid and structure (e.g. the added mass) can be fully considered.

5. Application: Green water slamming induced by freak wave

Freak wave, also called as rogue wave or monster wave, is a kind of extreme wave that has led to many destructions and accidents in recent decades (Kjeldsen, 1984; Lavrenov, 1998; Dysthe et al., 2008; etc.). When marine structures encounter with freak waves, green water and overtopping events are the most commonly observed consequences which might cause severe impact on superstructures (Qin et al., 2017a, 2017b, 2017c). Therefore, it is necessary to study the green water impact issue caused by freak waves, especially when hydroelastic effects cannot be neglected (Faltinsen et al., 1997). However, several problems are raised on the accuracy and efficiency balance of FSI simulation of this issue. Firstly, the relatively long simulation time of wave generation and propagation doesn't cohere with the transient simulation time of FSI. Secondly, the grid size of wave simulation which requires a relatively coarse grid to reduce computational cost doesn't cohere with the grid size of local FSI simulation which requires a fine grid to guarantee

accuracy. Thirdly, the small time step required by accurate calculation of high-frequency structural vibration doesn't cohere with the relatively large time step required by wave simulation, especially for monolithic FSI method. Lastly, solving the monolithic FSI equation in the whole domain brings unnecessary difficulty and costs too much time.

In this section, the green water impact on deck-house structures caused by freak waves are simulated using Concurrent Multi-Process Refinement method to conquer the problems listed before. This case shows the performance of Concurrent Multi-Process Refinement method in dealing with practical multi-scale ocean engineering problems including localized FSI simulations with high-frequency structural vibrations.

A numerical wave tank is built of 10 m in length, 1 m in height and 0.7 m in water-depth, where three gauges are placed 3 m (Gauge 1), 4 m (Gauge 2) and 5 m (Gauge 3) from the wave-making boundary. Freak waves based on Peregrine breather of nonlinear Schrödinger equation is applied (Akhmediev et al., 2009; Chabchoub et al., 2012; Hu et al., 2015; etc.), which is to reach the maximum crest at Gauge 2 at 10s with carrier wave number $k = 2.223\text{rad/m}$ and amplitude $A = 0.1\text{m}$. Physical properties within the fluid domain are chosen as: fluid density 1250 kg/m^3 , fluid kinematical viscosity $0.000001145\text{ m}^2/\text{s}$, air pressure 101263.4Pa , acceleration of gravity 9.81 m/s^2 . Before simulations of the interaction between freak wave and the platform, a verification on freak wave generation is conducted with the grid size of 0.02 m and time step of 0.002s. The numerical results of free surface elevations at Gauge 1, Gauge 2 and Gauge 3 are compared with the theoretical results in Fig. 17-a, showing satisfactory agreement.

The platform structure which is 1 m in length and 0.2 m in height is fixed 4 m from the wave-making boundary and 0.08 m above the still water line. On the platform, a 0.2 m-long clamped-clamped vertical wall is placed at the middle representing the deck-house wall, which is treated as a 0.001 m-thick elastic structure with elastic modulus 210 GPa, Poisson's ratio 0.3 and material density 7860 kg/m^3 . Three pressure monitors P_1 , P_2 and P_3 are located at the bottom, middle and top of the vertical wall.

The green water impact simulation is divided into three processes using Concurrent Multi-Process Refinement method, namely Main Process, Local Process A and Local Process B, grid sizes and time steps of which are given in Table 6. The vertical deck-house wall is discretized into 40 Euler beam elements. It should be noticed that the time step in Local Process B is 0.00005s, which is 1/20 of the time step in Local Process A due to the reason that the coupled FSI equation of Eq. (2.16) is solved in Local Process B. As mentioned before, in order to capture the high-frequency vibration of the elastic steel structures, solution of the monolithic FSI equation requires a much smaller time step compared to the ones in Main Process and Local Process A. The total simulation time of freak wave generation and propagation in Main Process is 20s, while the simulation times in Local Process A and Local Process B are both 1s.

Before the green water event occurs, the crest shape of the freak wave at 9.40s is shown in Fig. 17-b, indicating a nonlinear wave crest with a steep front and a gentle back. From 9.92s to 10.78s in which period the green water event lasts, the free surfaces and velocity vectors (black arrows) in Main Process, Local Process A and Local Process B are illustrated in Fig. 18. It is seen that with the refinement of multi-processes, the large-scale CFD wave simulation and the small-scale FSI simulation are well combined using Concurrent Multi-Process Refinement method. Nonlinear behaviors of fluid climbing, rolling, breaking and splashing are fully simulated in the small-scale FSI simulation in Local Process B, leading to more convincing loads on the elastic structure, and thus a more reliable hydroelastic response. Moreover, the small time step 0.00005s applied to solve the monolithic FSI equation is restricted within Local Process B, which significantly reduces the computational cost.

By the comparison among one-process, two-processes and three-processes, performance of Concurrent Multi-Process Refinement method can be seen from a series of contrast simulation tests listed in

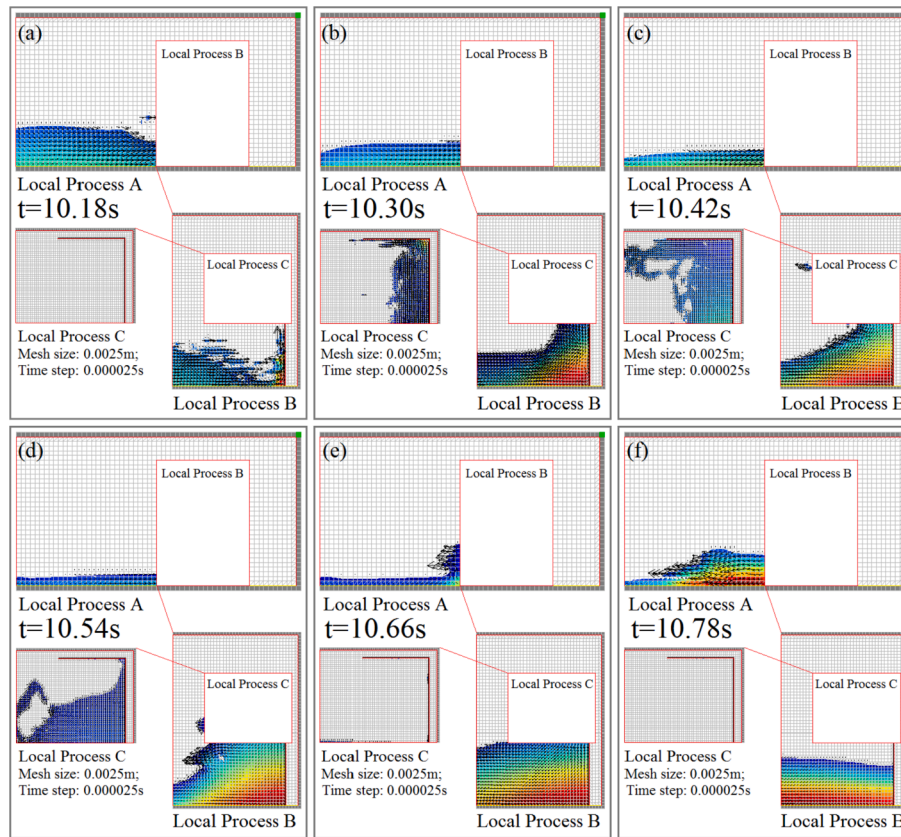


Fig. 20. Snapshots of the green water impact caused by freak wave in Local Process A, Local Process B and Local Process C using Concurrent Multi-Process Refinement method.

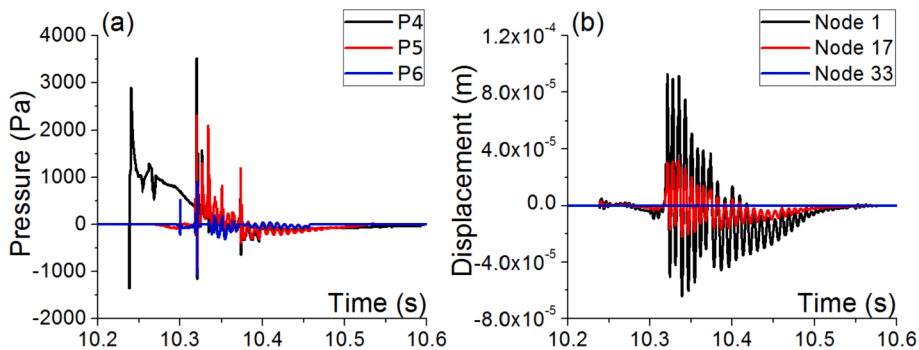


Fig. 21. Pressure time histories (Left Panel) and nodal displacements (Right Panel).

Table 9

Ratio between the added mass and the object mass.

Simulation case	Object	Object mass (kg/m)	Maximum added mass (kg/m)	R_{added}
Section 4.2	Vertical wall	14.34	25.79	1.80
Section 5	Vertical Wall	1.57	18.43	11.74
	Horizontal deck	0.94	2.06	2.19

Table 7. It is seen that directly applying a fine grid in one Main Process to guarantee the accuracy of local FSI simulation is computational expensive with over 100 h of simulation. By using a two-process division, computational cost can be reduced to 0.8 h of wave simulation and 2.3 h of FSI simulation, and thus a total cost of 3.1 h. However, the computational cost of using two-process division still overruns the cost of using

three-process division which is 1.8 h, consisting of 0.8 h of wave simulation and 0.1 h of green water simulation and 0.9 h of FSI simulation. Therefore, conclusion could be drawn that on condition of a reasonable division, Concurrent Multi-Process Refinement method improves the computational efficiency by applying more processes concurrently.

The pressure time histories at P_1 , P_2 and P_3 , and displacements of node 11, node 21 and node 31 of the wall are given in Fig. 19, from which the hydroelastic effects can be clearly observed through the oscillations of the pressures and displacements. As a result of FSI, vibration frequency of the vertical wall would be changing overtime with the impact of on-deck water. By using a Fast Fourier Transform (FFT), the vibration frequency of displacements and oscillation frequency of pressures are obtained, which vary from 37 Hz to 133 Hz, corresponding to a vibration period from 0.0270s to 0.0075s. From the lowest vibration and oscillation period, the reason of using a much smaller time step in

FSI simulations, which is 0.00005s in Local Process B (1/20 of the time step in Local Process A), can be reasonably explained as that only such small time step is able to capture the high-frequency structural vibrations and pressure oscillations. In other words, the usage of a much smaller time step in FSI simulations is determined by the high sampling frequency requirement of solving the monolithic FSI equation. However, in the fluid domain that is far away from the FSI area, the sampling frequency requirement of solving pure-CFD is much smaller, leading to the tolerance of using much larger time steps in Main Process and Local Process A according to the Courant number criterion.

Further considering the FSI problem of an elastic horizontal deck added at top of the deck-house wall, a four-process division is utilized by Concurrent Multi-Process Refinement method. The 0.08 m-long and 0.0015 m-thick horizontal deck is fixed at the right end and free at the left end, which is discretized into 32 Euler beam elements. Three pressure monitors P_4 , P_5 and P_6 are located at the right end, middle point and left end of the horizontal deck.

By further dividing Local Process B, the simulation is composed of Main Process, Local Process A, Local Process B and Local Process C, thus the FSI simulation solving the monolithic FSI equation is carried out in Local Process C. Grid sizes and time steps in Main Process, Local Process A, Local Process B and Local Process C are listed in Table 8. Snapshots of the events in Local Process A, Local Process B and Local Process C are illustrated in Fig. 20, from which the impact phenomena including violent fluid rolling, breaking, falling and splashing can be observed.

The pressure time histories at P_4 , P_5 and P_6 , and displacements of node 1, node 17 and node 33 of the deck are given in Fig. 21. By applying the FFT on displacement time histories, it is seen that the vibration frequency of the horizontal deck varies from 110 Hz to 196 Hz, corresponding to vibration period from 0.0091s to 0.0051s. From the lowest vibration period, it is seen that the sampling frequency requirement of the horizontal deck becomes even higher than the one of vertical wall due to a larger structural rigidity. Therefore, the simulation time step in solving the monolithic FSI equation should be further reduced, which is 0.000025s in Local Process C (1/2 of the time step in Local Process B). As a result, the computational cost using a four-process division is increased to 2.2 h, consisting of 0.8, 0.1 and 0.2 h of CFD simulations in Main Process, Local Process A and Local Process B, and 1.1 h of FSI simulation in Local Process C.

When dealing with multi-scale FSI problems such as the freak wave propagates, overtops in large-scale and causes slamming in small scale, the computational cost is usually high using the traditional monolithic FSI and refinement method. By reasonable division of the fluid domain, Concurrent Multi-Process Refinement method is able to save computational cost through multi-grid sizes and multi-time steps to multi-processes. As such, the scale differences between large-scale problems such as the wave propagation and overtopping, and small-scale problems such as the green water impact are well handled, leading to a well-balanced monolithic FSI simulation in accuracy and efficiency. However, as mentioned in Section 3.4 and Section 4.2, the division of multi-processes should be carefully chosen when dealing with multi-scale FSI problems to avoid under estimation of FSI effects, the added mass in particular.

6. Conclusions

In this paper, a Concurrent Multi-Process Refinement method applied in two-dimensional fluid-structure interaction problems is developed, which divides the FSI simulation into concurrent multi-processes with different grid sizes and time steps. As an important supplement of the SIMPLE-based monolithic implicit method (SBMIM) initially proposed by Hu et al. (2016), Concurrent Multi-Process Refinement method solves the accuracy and efficiency problems encountered during the implementation of the monolithic FSI method in dealing with multi-scale FSI problems and in predicting high-frequency structural vibrations.

By using the file mapping provided in Visual Basic, the split multi-processes are linked in pairs. In a pair of processes, data of velocity and pressure variables are transmitted between Main Process and Local Process through Fluid-Entry Boundary and Dummy Grid with proper interpolations and time advance strategy. The multi-grid sizes in Main Process and Local Process localize the FSI area so that the monolithic FSI equation can be solved in a limited scale, saving the computational cost induced by solution of the monolithic FSI equation. The multi-time steps in Main Process and Local Process balance the accuracy and efficiency temporally, especially under condition that a high sampling frequency is required to capture the high-frequency structural vibrations of large rigidity structures.

Two refinement study cases are given in the paper using the GCI method, including a case of the liquid sloshing in a baffled tank and a case of the dam breaking flow slamming a vertical wall. The liquid sloshing case shows the performance of Concurrent Multi-Process Refinement method in CFD simulations with nonlinear free surface evolutions, and gives an error estimation on the coarse, medium, fine and multi-process grids. The dam breaking case compares the results by present methods and by previous literatures, and gives an error estimation on different selected Local Process areas. Simulations of the green wave impact caused by a freak wave is conducted to show the practical application of Concurrent Multi-Process Refinement method in multi-scale FSI problems with high-frequency structural vibrations using monolithic FSI methods, from which it is seen that the present method can deal with ocean engineering problems composed of large-scale CFD issues such as the wave propagation and small-scale FSI issues such as the on-deck wave slamming. In addition, it is known that FSI coupling problems can well be explained by the fluid added mass in relation to the object mass, the ratio of which can determine whether a strong coupling is required or whether a weak coupling suffices. By using the FFT method, Table 9 gives the object mass, maximum added mass, and R_{added} (the ratio between maximum added mass and object mass), from which it can be observed that the added mass effect is quite severe in all the three FSI coupling simulations in this paper. This proves that the monolithically strong-coupled coupling method applied in this study is necessary and is able to give good results in evaluating the added mass effects.

The main innovation of the paper is the development of Concurrent Multi-Process Refinement method, which is based on a SIMPLE-based monolithic implicit method used for strong coupling FSI simulations. The novelty of Concurrent Multi-Process Refinement method lies in that it provides a solution of balancing the accuracy and efficiency in monolithic FSI methods, especially in dealing with multi-scale FSI problems and high-frequency structural vibrations. In addition, Concurrent Multi-Process Refinement method shows its great advantages in CFD/FSI simulations using low-cost computational facilities, making it possible for researchers to conduct time-costing monolithic FSI simulations using ordinary personal computers. Further study might be focused on the development of Concurrent Multi-Process Refinement method using adaptive meshing and time step, and the potential of parallel computation in multi-CPU.

Acknowledgement

This work was supported by the National Key Research and Development Program of China (Grant No. 2017YFC1404700), Key Special Project for Introduced Talents Team of Southern Marine Science and Engineering Guangdong Laboratory (Guangzhou) (Grant No. GML2019ZD0604), the Discipline Layout Project for Basic Research of Shenzhen Science and Technology Innovation Committee (Grant No. 20170418), the Guangdong Special Fund Program for Marine Economy Development (Grant No. GDME-2018E001).

The authors would like to thank the anonymous reviewers for their advisable comments.

References

- Afzal, A., Ansari, Z., Faizabadi, A.R., Ramis, M.K., 2017. Parallelization strategies for computational fluid dynamics software: state of the art review. *Arch. Comput. Methods Eng.* 24 (2), 337–363.
- Ahmed, N., John, V., 2015. Adaptive time step control for higher order variational time discretizations applied to convection–diffusion–reaction equations. *Comput. Methods Appl. Mech. Eng.* 285, 83–101.
- Akhmediev, N., Ankiewicz, A., Soto-Crespo, J.M., 2009. Rogue waves and rational solutions of the nonlinear Schrödinger equation. *Phys. Rev.* 80, 026601.
- Amritkar, A., Deb, S., Tafti, D., 2014. Efficient parallel CFD-DEM simulations using OpenMP. *J. Comput. Phys.* 256, 501–519.
- Basting, S., Quaini, A., Čanić, S., Glowinski, R., 2017. Extended ALE Method for fluid–structure interaction problems with large structural displacements. *J. Comput. Phys.* 331, 312–336.
- Bazilevs, Y., Takizawa, K., Tezduyar, T.E., 2013. *Computational Fluid-Structure Interaction: Methods and Applications*. John Wiley & Sons.
- Calandrini, S., Aulisa, E., 2019. Fluid-structure interaction simulations of venous valves: a monolithic ALE method for large structural displacements. *Int. J. Numer. Methods Biomed. Eng.* 35 (2), e3156.
- Celik, I.B., Ghia, U., Roache, P.J., Freitas, C.J., Coleman, H., Raad, P.E., 2008. Procedure for estimation and reporting of uncertainty due to discretization in CFD applications. *J. Fluids Eng. ASME* 130, 1–4. <https://doi.org/10.1115/1.2960953>, 078001.
- Chabchoub, A., Hoffmann, N., Onorato, M., Slunyaev, A., Sergeeva, A., Pelinovsky, E., Akhmediev, N., 2012. Observation of a hierarchy of up to fifth-order rogue waves in a water tank. *Phys. Rev. E* 86, 056601.
- Chen, Y., Luo, H., 2018. A computational study of the three-dimensional fluid–structure interaction of aortic valve. *J. Fluids Struct.* 80, 332–349.
- Cottet, G.H., Maitre, E., 2016. A semi-implicit level set method for multiphase flows and fluid–structure interaction problems. *J. Comput. Phys.* 314, 80–92.
- Crespo, A.J.C., Domínguez, J.M., Rogers, B.D., Gómez-Gesteira, M., Longshaw, S., Canelas, R., García-Feal, O., 2015. DualSPHysics: Open-source parallel CFD solver based on smoothed particle hydrodynamics (SPH). *Comput. Phys. Commun.* 187, 204–216.
- De Rosis, A., Ubertini, S., Ubertini, F., 2014. A partitioned approach for two-dimensional fluid–structure interaction problems by a coupled lattice Boltzmann-finite element method with immersed boundary. *J. Fluids Struct.* 45, 202–215.
- Dysthe, K., Krogstad, H.E., Müller, P., 2008. Oceanic rogue waves. *Annu. Rev. Fluid Mech.* 40 (1), 287–310.
- Faltinsen, O.M., Kvålsvold, J., Aarssen, J.V., 1997. Wave impact on a horizontal elastic plate. *J. Mar. Sci. Technol.* 2 (2), 87–100.
- Farhat, C., Lakshminarayan, V.K., 2014. An ALE formulation of embedded boundary methods for tracking boundary layers in turbulent fluid–structure interaction problems. *J. Comput. Phys.* 263, 53–70.
- Farhat, C., Lesoinne, M., 2000. Two efficient staggered algorithms for the serial and parallel solution of three-dimensional nonlinear transient aeroelastic problems. *Comput. Methods Appl. Mech. Eng.* 182 (3–4), 499–515.
- Farhat, C., Van der Zee, K.G., Geuzaine, P., 2006. Provably second-order time-accurate loosely-coupled solution algorithms for transient nonlinear computational aeroelasticity. *Comput. Methods Appl. Mech. Eng.* 195 (17–18), 1973–2001.
- Felippa, C.A., Park, K.C., Farhat, C., 2001. Partitioned analysis of coupled mechanical systems. *Comput. Methods Appl. Mech. Eng.* 190 (24–25), 3247–3270.
- Fenández-Tena, A., Marcos, A.C., Martínez, C., Keith Walters, D., 2017. A new adaptive time step method for unsteady flow simulations in a human lung. *Comput. Methods Biomech. Biomed. Eng.* 20 (8), 915–917.
- Förster, C., Wall, W.A., Ramm, E., 2007. Artificial added mass instabilities in sequential staggered coupling of nonlinear structures and incompressible viscous flows. *Comput. Methods Appl. Mech. Eng.* 196 (7), 1278–1293.
- Fourey, G., Hermange, C., Le Touzé, D., Oger, G., 2017. An efficient FSI coupling strategy between smoothed particle hydrodynamics and finite element methods. *Comput. Phys. Commun.* 217, 66–81.
- Godderidge, B., Tan, M., Turnock, S.R., Earl, C., 2006. A verification and validation study of the application of computational fluid dynamics to the modelling of lateral sloshing. *J. Eur. Ceram. Soc.* 28 (14), 2709–2716.
- Gropp, W.D., Kaushik, D.K., Keyes, D.E., Smith, B.F., 2001. High-performance parallel implicit CFD. *Parallel Comput.* 27 (4), 337–362, 2001.
- Heil, M., Hazel, A.L., Boyle, J., 2008. Solvers for large-displacement fluid–structure interaction problems: segregated versus monolithic approaches. *Comput. Mech.* 43 (1), 91–101.
- Heltai, L., Kiendl, J., DeSimone, A., Reali, A., 2017. A natural framework for isogeometric fluid–structure interaction based on BEM–shell coupling. *Comput. Methods Appl. Mech. Eng.* 316, 522–546.
- Houbolt, J.C., 1950. A recurrence matrix solution for the dynamic response of elastic aircraft. *J. Aeronaut. Sci.* 17 (9), 540–550.
- Hu, D., Long, T., Xiao, Y., Han, X., Gu, Y., 2014. Fluid–structure interaction analysis by coupled FE–SPH model based on a novel searching algorithm. *Comput. Methods Appl. Mech. Eng.* 276, 266–286.
- Hu, Z., Tang, W.Y., Xue, H.X., Zhang, X.Y., 2015. Numerical study of Rogue waves as nonlinear Schrödinger breather solutions under finite water depth. *Wave Motion* 52, 81–90.
- Hu, Z., Tang, W.Y., Xue, H.X., Zhang, X.Y., 2016. A SIMPLE-based monolithic implicit method for strong-coupled fluid–structure interaction problems with free surfaces. *Comput. Methods Appl. Mech. Eng.* 299, 90–115.
- Hübner, B., Walhorn, E., Dinkler, D., 2004. A monolithic approach to fluid–structure interaction using space–time finite elements. *Comput. Methods Appl. Mech. Eng.* 193 (23–26), 2087–2104.
- Hwang, S.C., Khayyer, A., Gotoh, H., Park, J.C., 2014. Development of a fully Lagrangian MPS-based coupled method for simulation of fluid–structure interaction problems. *J. Fluids Struct.* 50, 497–511.
- Hwang, S.C., Park, J.C., Gotoh, H., Khayyer, A., Kang, K.J., 2016. Numerical simulations of sloshing flows with elastic baffles by using a particle-based fluid–structure interaction analysis method. *Ocean Eng.* 118, 227–241.
- Ilie, M., 2018. Fluid-structure interaction in turbulent flows; a CFD based aeroelastic algorithm using LES. *Appl. Math. Comput.* <https://doi.org/10.1016/j.amc.2017.10.059>.
- John, D., Anderson, J.R., 1995. *Computational Fluid Dynamics: the Basics with Applications*. McGraw-Hill Book Company Europe, 1995.
- Johnson, D.E., 1966. A proof of the stability of the Houbolt method. *AIAA J.* 4 (8), 1450–1451.
- Jung, J.H., Yoon, H.S., Lee, C.Y., Shin, S.C., 2012. Effect of the vertical baffle height on the liquid sloshing in a three-dimensional rectangular tank. *Ocean Eng.* 44 (1), 79–89.
- Kamensky, D., Hsu, M.C., Schillinger, D., Evans, J.A., Aggarwal, A., Bazilevs, Y., Hughes, T.J., 2015. An immersed-geometric variational framework for fluid–structure interaction: application to bioprosthetic heart valves. *Comput. Methods Appl. Mech. Eng.* 284, 1005–1053.
- Kjeldsen, S.P., 1984. Dangerous wave groups. *Nor. Marintime Res.* 2, 4–16.
- Küttler, U., Wall, W.A., 2008. Fixed-point fluid–structure interaction solvers with dynamic relaxation. *Comput. Mech.* 43 (1), 61–72.
- Lavrenco, I.V., 1998. The wave energy concentration at the Agulhas current off South Africa. *Nat. Hazards* 17 (2), 117–127.
- Le Tallec, P., Mouro, J., 2001. Fluid structure interaction with large structural displacements. *Comput. Methods Appl. Mech. Eng.* 190 (24–25), 3039–3067.
- Li, Z., Leduc, J., Nunez-Ramirez, J., Combesure, A., Marongiu, J.C., 2015. A non-intrusive partitioned approach to couple smoothed particle hydrodynamics and finite element methods for transient fluid–structure interaction problems with large interface motion. *Comput. Mech.* 55 (4), 697–718.
- Lin, P., 2007. A fixed-grid model for simulation of a moving body in free surface flows. *Comput. Fluids* 36 (3), 549–561.
- Liu, X., Xu, H., Shao, S., Lin, P., 2013. An improved incompressible SPH model for simulation of wave–structure interaction. *Comput. Fluids* 71, 113–123.
- Liu, J., Jaiman, R.K., Gurugubelli, P.S., 2014. A stable second-order scheme for fluid–structure interaction with strong added-mass effects. *J. Comput. Phys.* 270, 687–710.
- Löhner, R., 2001. *Adaptive Mesh Refinement. Applied Computational Fluid Dynamics Techniques: an Introduction Based on Finite Element Methods*, second ed., pp. 269–297.
- Matthies, H.G., Steindorf, J., 2003. Partitioned strong coupling algorithms for fluid–structure interaction. *Comput. Struct.* 81 (8–11), 805–812.
- Mitsume, N., Yoshimura, S., Murotani, K., Yamada, T., 2014. MPS–FEM partitioned coupling approach for fluid–structure interaction with free surface flow. *Int. J. Comput. Methods* 11 (04), 1350101.
- Newmark, N.M., 1959. *A Method of Computation for Structural Dynamics*. American Society of Civil Engineers.
- Nickel, R.E., 1971. On the stability of approximation operators in problems of structural dynamics. *Int. J. Solids Struct.* 7 (3), 301–319.
- Park, S., Oh, G., Rhee, S.H., Koo, B.Y., Lee, H., 2015. Full scale wake prediction of an energy saving device by using computational fluid dynamics. *Ocean Eng.* 101, 254–263.
- Patankar, S.V., Spalding, D.B., 1972. A calculation procedure for heat, mass and momentum transfer in three-dimensional parabolic flows. *Int. J. Heat Mass Transf.* 15 (10), 1787–1806.
- Plewa, T., Linde, T., Weirs, V.G., Numerik, 2005. *Adaptive Mesh Refinement - Theory and Applications*. Springer Berlin Heidelberg.
- Qin, H., Tang, W.Y., Xue, H.X., Hu, Z., 2017a. Dynamic response of a horizontal plate dropping onto nonlinear freak waves using a fluid–structure interaction method, 2017 *J. Fluids Struct.* 74.
- Qin, H., Tang, W.Y., Hu, Z., Guo, J.T., 2017b. Structural response of deck structures on the green water event caused by freak waves. *J. Fluids Struct.* 68, 322–338.
- Qin, H., Tang, W.Y., Xue, H.X., Hu, Z., Guo, J.T., 2017c. Numerical study of wave impact on the deck-house caused by freak waves. *Ocean Eng.* 133, 151–169.
- Ravník, J., Strelnikova, E., Gnitko, V., Degtyarev, K., Ogorodnyk, U., 2016. BEM and FEM analysis of fluid–structure interaction in a double tank. *Eng. Anal. Bound. Elem.* 67, 13–25.
- Richardson, L.F., 1911. IX. The approximate arithmetical solution by finite differences of physical problems involving differential equations, with an application to the stresses in a masonry dam. *Phil. Trans. R. Soc. Lond. A* 210 (459–470), 307–357.
- Richter, T., 2013. A fully Eulerian formulation for fluid–structure-interaction problems. *J. Comput. Phys.* 233, 227–240.
- Roache, P.J., 2003. Conservatism of the grid convergence index in finite volume computations on steady-state fluid flow and heat transfer. *J. Fluids Eng.* 125 (4), 731–732.
- Rodríguez-Tembleque, L., González, J.A., Cerrato, A., 2015. Partitioned solution strategies for coupled BEM–FEM acoustic fluid–structure interaction problems. *Comput. Struct.* 152, 45–58.
- Sun, Z., Djidjeli, K., Xing, J.T., 2015. Modified MPS method for the 2D fluid structure interaction problem with free surface. *Comput. Fluids* 122, 47–65.
- Takizawa, K., Tezduyar, T.E., 2011. Multiscale space–time fluid–structure interaction techniques. *Comput. Mech.* 48 (3), 247–267.
- Timoshenko, S., Woinowsky-Krieger, S., 1959. *Theory of Plates and Shells*. McGraw-Hill, New York.

- Torii, R., Oshima, M., Kobayashi, T., Takagi, K., Tezduyar, T.E., 2009. Fluid–structure interaction modeling of blood flow and cerebral aneurysm: significance of artery and aneurysm shapes. *Comput. Methods Appl. Mech. Eng.* 198 (45–46), 3613–3621.
- Wick, T., 2013. Fully Eulerian fluid–structure interaction for time-dependent problems. *Comput. Methods Appl. Mech. Eng.* 255, 14–26.
- Wu, Y., Cai, X.C., 2014. A fully implicit domain decomposition based ALE framework for three-dimensional fluid–structure interaction with application in blood flow computation. *J. Comput. Phys.* 258, 524–537.
- Yang, Q., 2011. SPH Simulation of Fluid-Structure Interaction Problems with Application to Hovercraft. Doctoral dissertation. Virginia Tech.
- Yao, W., Marques, S., 2017. Application of a high-order CFD harmonic balance method to nonlinear aeroelasticity. *J. Fluids Struct.* 74, 427–444.
- Youngs, D.L., 1982. Time-dependent multi-material flow with large fluid distortion. In: Morton, K.W., Baines, M.J. (Eds.), *Numerical Methods for Fluid Dynamics*. Academic Press.
- Zhang, Y., Wan, D., 2018. MPS-FEM coupled method for sloshing flows in an elastic tank. *Ocean Eng.* 152, 416–427.
- Zhang, A.M., Ming, F.R., Wang, S.P., 2013. Coupled SPHS–BEM method for transient fluid–structure interaction and applications in underwater impacts. *Appl. Ocean Res.* 43, 223–233.